JBC RESEARCH ARTICLE

A minimal construct of nuclear-import receptor Karyopherin-β2 defines the regions critical for chaperone and disaggregation activity

Received for publication, September 19, 2022, and in revised form, December 2, 2022 Published, Papers in Press, December 15, 2022,
https://doi.org/10.1016/j.jbc.2022.102806

Charlotte M. Fare[1,2], **Kevin Rhine**[3,4], **Andrew Lam**[1], **Sua Myong**[3,4], **and James Shorter**[1,2,*]

From the [1]*Department of Biochemistry and Biophysics, and* [2]*Biochemistry and Molecular Biophysics Graduate Group, Perelman School of Medicine at the University of Pennsylvania, Philadelphia, Pennsylvania, USA;* [3]*Program in Cell, Molecular, Developmental Biology, and Biophysics, and* [4]*Department of Biophysics, Johns Hopkins University, Baltimore, Maryland, USA*

Edited by Ursula Jakob

Karyopherin-β2 (Kapβ2) is a nuclear-import receptor that recognizes proline-tyrosine nuclear localization signals of diverse cytoplasmic cargo for transport to the nucleus. Kapβ2 cargo includes several disease-linked RNA-binding proteins with prion-like domains, such as FUS, TAF15, EWSR1, hnRNPA1, and hnRNPA2. These RNA-binding proteins with prion-like domains are linked *via* pathology and genetics to debilitating degenerative disorders, including amyotrophic lateral sclerosis, frontotemporal dementia, and multisystem proteinopathy. Remarkably, Kapβ2 prevents and reverses aberrant phase transitions of these cargoes, which is cytoprotective. However, the molecular determinants of Kapβ2 that enable these activities remain poorly understood, particularly from the standpoint of nuclear-import receptor architecture. Kapβ2 is a super-helical protein comprised of 20 HEAT repeats. Here, we design truncated variants of Kapβ2 and assess their ability to antagonize FUS aggregation and toxicity in yeast and FUS condensation at the pure protein level and in human cells. We find that HEAT repeats 8 to 20 of Kapβ2 recapitulate all salient features of Kapβ2 activity. By contrast, Kapβ2 truncations lacking even a single cargo-binding HEAT repeat display reduced activity. Thus, we define a minimal Kapβ2 construct for delivery in adeno-associated viruses as a potential therapeutic for amyotrophic lateral sclerosis/frontotemporal dementia, multisystem proteinopathy, and related disorders.

Karyopherin-β2 (Kapβ2; also known as Transportin 1) is a nuclear-import receptor (NIR) that transports proteins bearing a proline-tyrosine nuclear localization signal (PY-NLS) from the cytoplasm to the nucleus (1–4). Kapβ2, like other NIRs, promotes nuclear import based on the presence of an asymmetric Ran gradient (3, 5). Ran is a small GTPase, and its GTPase-activating protein, RanGAP1, is restricted to the cytoplasm, whereas its guanine-nucleotide-exchange factor, RCC1, is localized to the nucleus (3, 5). Thus, Ran-GDP is predominant in the cytoplasm, whereas Ran-GTP is predominant in the nucleus (3, 5, 6). Kapβ2 has a low affinity for Ran-GDP, which permits Kapβ2 interactions with cargo in the cytoplasm (3, 7). Once in the nucleus, Kapβ2 is engaged tightly by Ran-GTP, which elicits a conformational change in Kapβ2 that releases cargo and liberates Kapβ2 for repeated rounds of nuclear import (3, 7–10).

The best-characterized class of cargo recognized by Kapβ2 are proteins bearing a PY-NLS (1, 2, 11–14). The PY-NLS is defined by three distinct epitopes that each contribute to cargo-recognition. A hydrophobic or basic motif is epitope 1, which is followed by a R-X_{2-5}-PY motif where R-X_{2-5} is epitope 2 and the C-terminal PY is epitope 3 (1, 12, 13). Kapβ2 was initially described with respect to its role in nuclear import (7, 10, 11, 15). More recently, Kapβ2 has been defined as a potent molecular chaperone that can prevent and reverse aberrant phase transitions of its specific cargo (16–24).

The newly appreciated chaperone and disaggregation activity of Kapβ2 could have therapeutic utility (6, 25–28). Indeed, several of the cargo recognized by Kapβ2 are prominent RNA-binding proteins (RBPs) with prion-like domains (PrLDs), which are connected to neurodegenerative disease *via* both pathology and genetics, including FUS, hnRNPA1, hnRNPA2, TAF15, and EWSR1 (8, 10, 11, 15, 16, 29–34). In particular, mutations in genes encoding RBPs with PrLDs can cause amyotrophic lateral sclerosis (ALS), frontotemporal dementia (FTD), multisystem proteinopathy (MSP), oculopharyngeal muscular dystrophy, hereditary motor neuropathy, and related disorders (35–42). In the postmortem brain tissue of ALS/FTD patients, specific nuclear RBPs with PrLDs have been found to be depleted from the nucleus and mislocalized and aggregated in the cytoplasm of degenerating neurons (37, 38, 43–49). The manner by which cytoplasmic mislocalization of specific RBPs with PrLDs elicits neurodegeneration has two dimensions: (1) RBPs play an essential role in RNA metabolism (28, 45, 50–52), and their cytoplasmic mislocalization may elicit loss-of-function phenotypes that contribute to toxicity; and (2) the insoluble cytoplasmic forms of these RBPs may be intrinsically toxic (43, 53–58), indicating a gain-of-function mechanism of toxicity.

Despite the potential risk of forming toxic assemblies, the ability for RBPs to self-assemble into phase-separated states

* For correspondence: James Shorter, jshorter@pennmedicine.upenn.edu.

also has biological utility (28, 59–61). RBPs with PrLDs can mediate multivalent intermolecular contacts, allowing them to self-associate and condense into phase-separated bodies (28, 56, 59, 62–65). In particular, RBPs with PrLDs like FUS and hnRNPA1 partition into stress granules (SGs), phase-separated membrane-less organelles that form in the cytoplasm in response to stress (16, 28, 39, 56, 63, 66–69). Dysregulation of SGs has been implicated in the appearance of cytoplasmic aggregates, which are associated with the development of ALS/FTD and MSP (31, 39, 56, 63, 70–72). Indeed, liquid condensates formed by RBPs with PrLDs can mature into pathological solid phases comprised of cross-β fibrils that are associated with disease, and this process is often accelerated by disease-linked mutations (20, 56, 70, 73). Ensuring that RBPs do not get trapped in toxic pathological phases is a problem that all cells must solve (25, 26, 28).

Cells have evolved agents to dissolve aberrant protein states, including NIRs (6, 25, 26). *In vitro*, Kapβ2 prevents and reverses the formation liquid-like condensates, dense hydrogels, and solid-like fibrils formed by RBP cargo, including FUS and hnRNPA1 (16–22, 24). Moreover, Kapβ2 performs these activities *in vivo* to antagonize the formation of cytoplasmic RBP aggregates, restore functional RBPs to the nucleus, and mitigate disease-linked RBP toxicity (6, 16, 27). Thus, by combining chaperone and nuclear-import activities, Kapβ2 antagonizes cytoplasmic RBP aggregation and the loss of RBP function in the nucleus (16).

In addition to recognizing cargo with a PY-NLS, Kapβ2 exhibits NLS-independent chaperone activity (27, 74). For example, Kapβ2 can antagonize aberrant phase transitions and interactions of ALS/FTD-associated nonnative poly(GR) and poly(PR) dipeptide-repeat proteins produced by repeat-associated non-AUG translation of the pathogenic G_4C_2 hexanucleotide repeat expansion in the *C9ORF72* gene (27, 74–77). This Kapβ2 activity is neuroprotective (78). Kapβ2 mediates this chaperone activity by interacting with arginine residues, a strategy that is employed by a host of NIRs to chaperone a network of native and mutant clients (22, 23).

Kapβ2 chaperone activity is limited by its affinity for cargo. Kapβ2 typically recognizes cargo with nanomolar affinity (1, 12, 14, 23). Two tryptophan residues, W460 and W730, on the cargo-binding surface of Kapβ2 play a critical role in cargo recognition, as they participate in hydrophobic sidechain stacking interactions with the PY-NLS (1). Importantly, a mutant form of Kapβ2, Kapβ2$^{W460A:W730A}$, which has reduced affinity for PY-NLS–bearing cargo displays reduced chaperone activity (1, 16).

Mutations that affect the PY-NLS or the biophysical properties of its cargo can also reduce Kapβ2 function (16, 20, 41). PY-NLS mutations can be particularly devastating and cause juvenile ALS, as with FUS^{P525L}, where the conserved proline of the PY-NLS is mutated to leucine (79, 80). Such aggressive pathology is explained at the molecular level, as Kapβ2 can have significantly lower affinity for PY-NLS mutant protein (14, 16, 17, 23, 81). Kapβ2 does show activity against PY-NLS mutants, but higher Kapβ2 concentrations are required for robust effects (16, 19, 23). Moreover, mutations outside of the PY-NLS can hamper Kapβ2 activity. For example, when Kapβ2 is added to self-assembled FUS harboring–specific disease-linked mutations outside the PY-NLS that reduce the dynamics of FUS self-assembly, it can only partially restore WT FUS-like behavior (20, 24). Thus, even when a cargo PY-NLS is intact, other more distributed secondary interactions are critical for Kapβ2 chaperone activity (16, 19). Beyond these insights, however, it remains unclear how Kapβ2 chaperones and disaggregates its cargo.

Here, to probe the mechanism by which Kapβ2 chaperones cargo, we rationally design truncated variants of Kapβ2 and assess their activity. Specifically, we assess their ability to (1) antagonize FUS aggregation and toxicity in yeast, (2) antagonize FUS condensation at the pure protein level, and (3) antagonize FUS condensation in human cells. We find that a C-terminal fragment of Kapβ2 that contains all cargo-binding residues can perform chaperone activity *in vitro* and can chaperone FUS in yeast and human cells to a similar extent as Kapβ2. At a minimum, our findings illuminate key mechanistic aspects of Kapβ2 chaperone activity with respect to NIR architecture. Moreover, we reveal a minimal Kapβ2 construct that might be more readily delivered in adeno-associated viruses (AAVs) as a potential therapeutic for several debilitating degenerative disorders.

Results

Designing truncated Kapβ2 variants to define the molecular determinants of chaperone activity

Kapβ2 combines cargo recognition and nuclear delivery in a single NIR (6, 82). Kapβ2 is a super-helical protein that is comprised of 20 HEAT (Huntington, Elongation factor 3, A subunit of protein phosphatase 2A, and Tor1 kinase) repeats (83). Each HEAT repeat is a protein tandem repeat structural motif (∼30–40 residues) composed of two antiparallel alpha helices (referred to as A- and B-helices) that are typically connected by a short loop (84). The super-helical conformation of Kapβ2 is found in the unbound state and when Kapβ2 is bound to Ran-GTP or FUS PY-NLS cargo (14, 83, 85) (Fig. 1*A*). Comparing the crystal structure of unbound Kapβ2 with that of Ran-GTP–bound and cargo (FUS PY-NLS)–bound Kapβ2 reveals three functionally distinct segments (86). An N-terminal segment (N1) consisting of HEAT repeats 1 to 8 (H1-H8) interacts with Ran-GTP in the nucleus to facilitate cargo release (86) (Fig. 1*A*). In the cytoplasm, two C-terminal segments, H9-H13 (C1) and H14-H18 (C2), rotate about a flexible hinge in H13-H14 in response to cargo loading (7, 83, 86) (Fig. 1*A*). In the unbound state, N-terminal H1-H4 and C-terminal H19-H20 exhibit flexibility (86).

Each segment of Kapβ2 contains residues that engage PY-NLS epitopes (1, 86). H8 of N1 and H9-H10 of C1 interact with the PY residues of epitope 3, H11-H13 of C1 and H14 of C2 interact with epitope 2, and H14-H17 of C2 interact with the hydrophobic/basic epitope 1 (1, 14, 86) (Fig. 1, *B* and *C*). The energetic importance of each epitope of the PY-NLS for Kapβ2 binding varies across different cargo, and so the extent

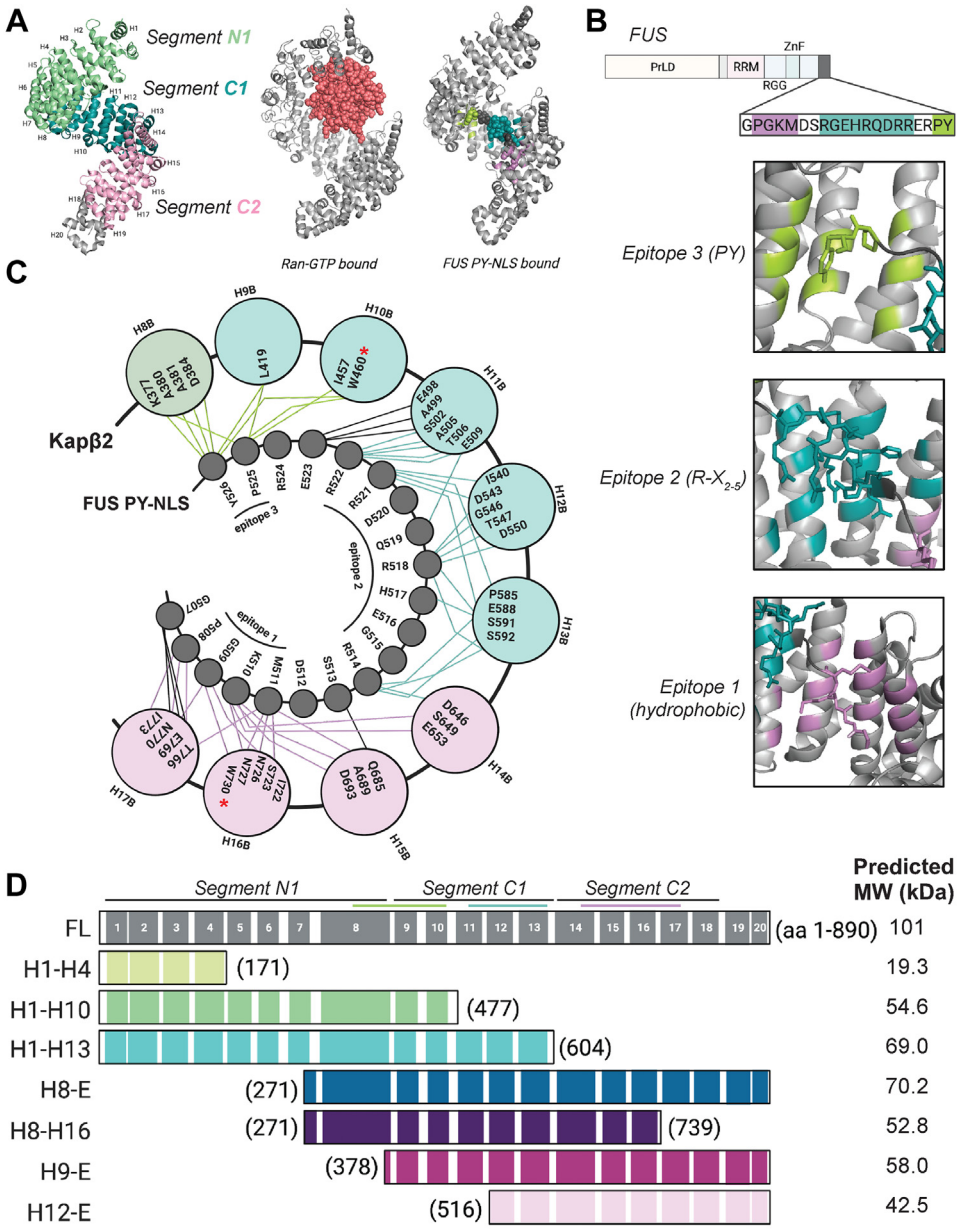

Figure 1. Binding of Kapβ2 to the PY-NLS of FUS is segmental. *A*, *left*, a crystal structure of Kapβ2 in its unbound state (PDB: 2QMR) with each HEAT repeat indicated. Each structural segment is colored: N-terminal segment, N1 (*green*), the first C-terminal segment, C1 (*teal*), and the second C-terminal segment, C2 (*light pink*). *Middle*, a structure of Kapβ2 in its Ran-GTP bound state, where Kapβ2 is *gray* and Ran-GTP is *salmon* (PDB: 1QBK). *Right*, Kapβ2 is shown bound to the PY-NLS of FUS, where epitope 1 is *lilac*, epitope 2 is *teal*, and epitope 3 is *lime* (PDB: 4FDD). Kapβ2 adopts a largely similar structure in all three states, with slight variations at the N- and C-terminal segments to accommodate binding partners. *B*, *top*, the domain architecture of FUS, with the PY-NLS sequence highlighted. FUS harbors an N-terminal prion-like domain (PrLD), followed by an RNA-recognition motif (RRM), an Arg-Gly-Gly-rich (RGG) domain, a zinc finger (ZnF), and a second RGG domain. *Bottom*, zoomed-in images of each epitope of the FUS PY-NLS bound to Kapβ2. The residues of Kapβ2 that contact the PY-NLS are colored corresponding to which epitope they interact with, where epitope 3 contacts are colored in *lime*, epitope 2 contacts are *teal*, and epitope 1 contacts are *lilac*. *C*, a cartoon depiction of Kapβ2 bound to the PY-NLS of FUS, where the *outer circles* represent each interior (*B*) helix of the indicated HEAT repeat and the *inner circles* represent the residues of the FUS PY-NLS. The *outer circles* are color-coded according by which segment they belong to, with segment N1 shown in *green*, segment C1 shown in *teal*, and segment C2 shown in *pink*. Interactions between Kapβ2 and FUS are shown as lines connecting Kapβ2 residues and FUS residues. *Lines* are colored to indicate residues making epitope contacts, where epitope 3 contacts are colored in *lime*, epitope 2 contacts are *teal*, and epitope 1 contacts are *lilac*. When Kapβ2 binds to FUS and other cargo, stereotypic residues within the inner helix of each HEAT repeat contact distinct cargo epitopes. W460 and W730, which are mutated to alanine in Kapβ2$^{W460A:W730A}$, are indicated with *red asterisks*. *D*, *top*, a diagram of Kapβ2 with specific structural features highlighted. The *black lines* indicate the HEAT repeats (shown as numbered *gray boxes*) comprising the N1, C1, and C2 segments; the *lime*, *teal*, and *lilac* lines indicate the regions of Kapβ2 that interact with epitope 3, 2, and 1, respectively. *Bottom*, a diagram of each truncation investigated here, named for the HEAT repeats contained in the construct including the amino acids (aa) contained in each construct, and the predicted molecular weight (MW). HEAT, Huntington, Elongation factor 3, A subunit of protein phosphatase 2A, and Tor1 kinase; Kapβ2, Karyopherin-β2; PY-NLS, proline-tyrosine nuclear localization signal.

to which Kapβ2 depends on the recognition of any specific epitope for a given cargo protein can be difficult to assess *a priori* (1, 12, 83, 86, 87). However, there are key interactions that appear critical for many cargoes, such as the interactions with epitopes 1 and 3 that are impacted by the Kapβ2$^{W460A:W730A}$ mutant (1, 16).

To determine the role of each of the larger structural elements of Kapβ2 with respect to chaperone activity, we designed seven truncated Kapβ2 constructs that span the length of the protein (Fig. 1*D*). The truncations were designed to probe the importance of the distribution of Kapβ2 residues that contact cargo, paying special attention to the residues that make direct contact with the PY epitope of the PY-NLS (1, 12, 14, 87).

First, H1-H4 (residues 1–171) was designed to test the N-terminal region of Kapβ2 (Fig. 1*D*). This region engages Ran-GTP but is not known to engage FUS (Fig. 1*A*). Hence, we do not anticipate this construct will have chaperone activity.

Second, H1-H10 (residues 1–477) contains segment N1 and the two N-terminal HEAT repeats of segment C1, which contain all the residues that interact with the PY-epitope of FUS, including W460 (Fig. 1, *C* and *D*). If H1-H10 can chaperone FUS as effectively as Kapβ2, then recognition of the PY-epitope alone would be sufficient for chaperone activity.

Third, H1-H13 (residues 1–604) contains segments N1 and C1 which contain the residues that engage epitopes 2 and 3 (Fig. 1, *C* and *D*). If H1-H13 can chaperone FUS as effectively as Kapβ2, then recognition of epitopes 2 and 3 would be sufficient for chaperone activity.

Fourth, H8-E (HEAT repeat 8 to end; residues 271–890) harbors HEAT repeat 8 from N1 plus both C-terminal segments which contain all the residues that contact each epitope of the FUS PY-NLS (Fig. 1, *C* and *D*). If H8-E can chaperone FUS as effectively as Kapβ2, then recognition of epitopes 1, 2, and 3 would be sufficient for chaperone activity.

Fifth, H8-H16 (residues 271–739) harbors a subset of the residues that interact with epitope 1 and all the residues that contact epitope 2 and 3, including W730 (Fig. 1, *C* and *D*). If H8-H16 can chaperone FUS as effectively as Kapβ2, then partial recognition of epitope 1 plus contacts with epitope 2 and 3 would be sufficient for chaperone activity.

Sixth, H9-E (residues 378–890) contains segment C1 and C2 and contacts both residues of the PY-epitope, albeit less extensively than H8-E, and contains all contacts for epitopes 1 and 2 (Fig. 1, *C* and *D*). If H9-E can chaperone FUS as effectively as Kapβ2, then partial recognition of epitope 3 plus contacts with epitope 1 and 2 would be sufficient for chaperone activity.

Seventh, H12-E (residues 516–890) contains part of segment C1 and all of segment C2, thereby retaining all the contacts for epitope 1 and a subset of contacts for epitope 2 (Fig. 1, *C* and *D*). If H12-E can chaperone FUS as effectively as Kapβ2, then the PY-epitope would be dispensable for Kapβ2 to chaperone cargo. We do not expect this possibility given the importance of the PY-epitope integrity for human health (16, 23, 41, 48, 79, 80). Collectively, this set of Kapβ2 truncations will enable us to define structural and sequence characteristics of Kapβ2 that are critical for its chaperone activity.

A C-terminal fragment of Kapβ2, H8-E, mitigates FUS toxicity in yeast

To determine whether truncated Kapβ2 proteins retain chaperone activity, we expressed each construct in a yeast model of FUS proteinopathy. For these studies, we utilized a yeast strain lacking Hsp104, a powerful protein disaggregase that is not found in humans (26, 88–91). Overexpression of FUS in this system elicits cytoplasmic FUS aggregation and toxicity, thereby mimicking phenotypes of degenerating neurons in ALS/FTD with FUS pathology (35, 92–94). Indeed, elevated FUS expression is linked to ALS (95, 96). Our yeast model of FUS proteinopathy has illuminated several genetic modifiers of FUS aggregation and toxicity, which have translated to fly, mammalian cell, and neuronal models of ALS/FTD (16, 18, 92–94, 97–102). Additionally, the yeast homolog of Kapβ2, Kap104, does not engage FUS effectively and cannot transport FUS into the nucleus, providing a simple system for measuring the specific activity of Kapβ2 (13, 16, 92, 93).

First, we tested whether expression of the Kapβ2 constructs on their own was toxic in yeast. Generally, the Kapβ2 constructs were not overtly toxic (Fig. S1*A*). Unexpectedly, however, H1-H10 exhibited some toxicity as did H8-E to a lesser extent (Fig. S1*A*). Next, we tested whether truncated forms of Kapβ2 could mitigate FUS toxicity in yeast. Full-length (FL), WT Kapβ2 mitigates FUS toxicity in yeast (Fig. 2*A*) without affecting FUS expression levels (Fig. 2*B*). Of the Kapβ2 truncations tested here, those which lack the complete set of FUS-interacting residues (Fig. 1, *C* and *D*) did not mitigate FUS toxicity (Fig. 2*A*). Thus, H1-H4 (no FUS-binding residues), H1-H10 (lacks epitope 1– and 2–binding residues), H1-H13 (lacks epitope 1-binding residues), H8-H16 (lacks epitope 1-binding residues in H17), H9-E (lacks epitope 3-binding residues in H8), and H12-E (lacks epitope 2– and 3–binding residues in H8-H11) did not mitigate FUS toxicity (Figs. 1*C* and 2*A*). Perhaps most surprising was the ineffectiveness of H9-E and H8-16, each of which only lack a few FUS-binding residues and retain both W460 and W730 (Fig. 1*C*). Thus, the absence of even a few FUS-binding residues reduces the ability of Kapβ2 to mitigate FUS toxicity in yeast.

We also tested Kapβ2$^{W460A:W730A}$ (Fig. S1, *B*–*D*), which has just two FUS-binding residues mutated. Kapβ2$^{W460A:W730A}$ was slightly toxic when expressed alone in yeast (Fig. S1*D*). Kapβ2$^{W460A:W730A}$ was unable to effectively mitigate FUS toxicity, despite being expressed at similar levels to Kapβ2 (Fig. S1, *B* and *C*). Thus, mutating just two residues in Kapβ2 that engage epitope 1 (W730) and epitope 3 (W460) of the FUS-PY-NLS reduces Kapβ2 activity (16).

In contrast, an N-terminal Kapβ2 truncation that begins at H8 (H8-E, residues 271–890; Fig. 1*D*) mitigates FUS toxicity without affecting FUS expression level (Fig. 2, *A* and *B*). H8-E is the only truncation tested here that contains all the Kapβ2 residues that bind the FUS PY-NLS, as well as the acidic loop in H8, which is necessary for cargo release in the nucleus (1, 12, 14). Our findings suggest that the entire cargo-binding surface of Kapβ2 is required for Kapβ2 to mitigate FUS toxicity in yeast.

There are several possible explanations for why an N- or C-terminally truncated Kapβ2 construct might not mitigate FUS toxicity despite retaining the residues known to contact each epitope of the PY-NLS, including the critical Trp residues at positions 460 and 730. For example, a truncated construct may

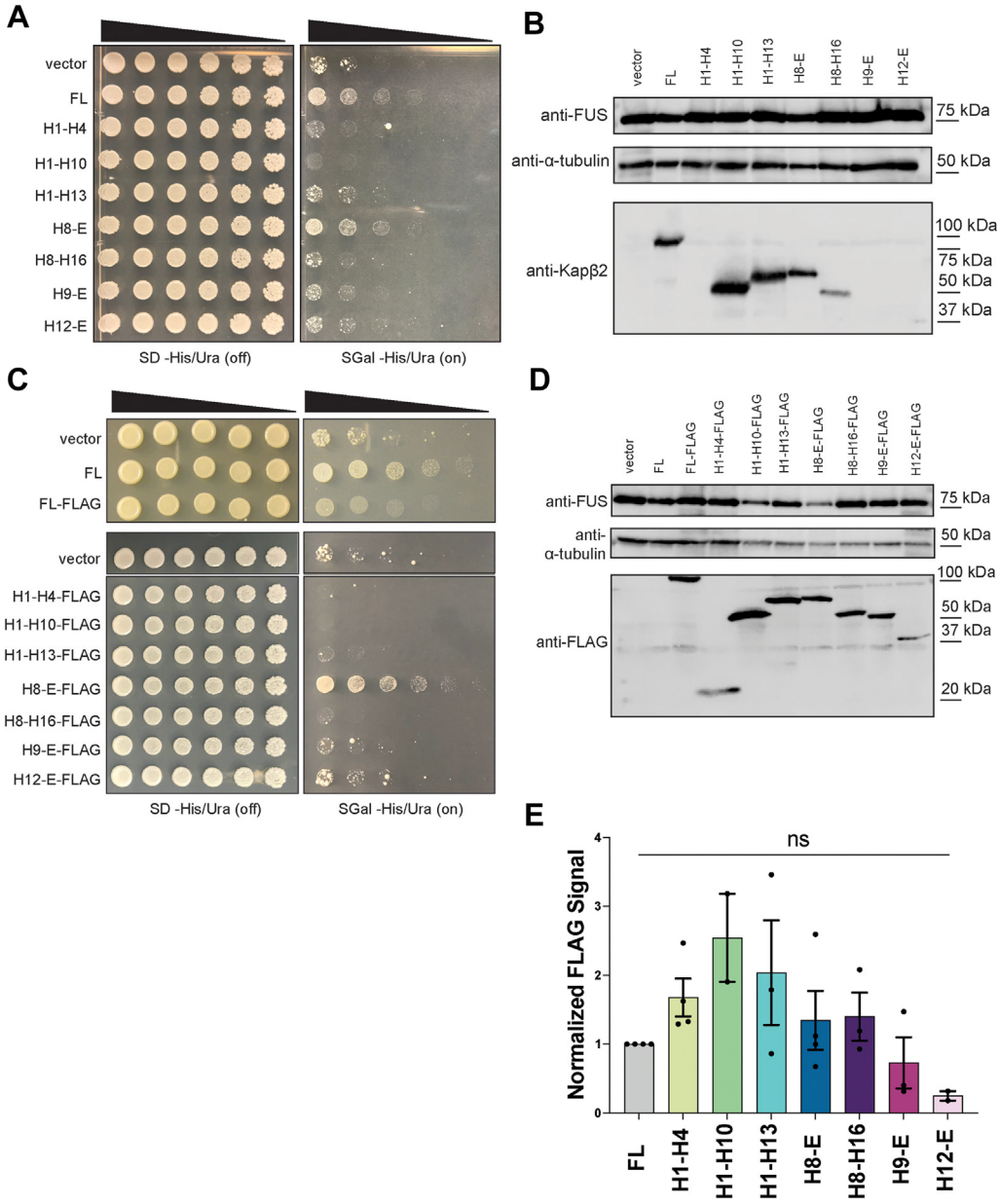

Figure 2. Kapβ2 and H8-E mitigate FUS toxicity in yeast. *A*, Δ*hsp104* yeast with galactose-inducible FUS integrated were transformed with the indicated galactose-inducible Kapβ2 construct and serially diluted 3-fold onto agar plates with either glucose (expression off) or galactose (expression on) as the carbon source. In the absence of Kapβ2 (vector), FUS expression is very toxic. This toxicity can be mitigated by the expression of full-length (FL) Kapβ2. Growth is also restored with the expression of a C-terminal fragment, H8-E. None of the other Kapβ2 truncations mitigate FUS toxicity. *B*, Western blot showing FUS and Kapβ2 expression for each condition. The Kapβ2 antibody recognizes residues 298 to 389 in the eighth HEAT repeat, and thus H1-H4, H9-E, and H12-E are not recognized. However, FUS expression is equal in all conditions as compared to the loading control, α-tubulin. *C*, FLAG-tagged Kapβ2 constructs were transformed into Δ*hsp104* yeast with integrated galactose-inducible FUS and serially diluted 3-fold onto agar plates with either glucose or galactose as the carbon source. FL Kapβ2-FLAG and H8-E-FLAG suppress FUS toxicity, whereas other Kapβ2 truncations do not. *D*, a Western blot illustrates that most truncations are expressed to similar levels, with H12-E showing slightly lower expression relative to the loading control, α-tubulin. *E*, Western blots were quantified by first normalizing the intensity of the FLAG band to the intensity of the loading control, α-tubulin. The ratio for FL Kapβ2 was then set as 1, and all other values were normalized to FL. H1-H4, H1-H10, and H1-H13 each show somewhat higher levels of expression, whereas H9-E and H12-E show somewhat lower levels of expression. Data points represent individual blots, bars represent means ± SD, n = 2 to 4. An ordinary one-way ANOVA with Tukey's multiple comparisons test was used to compare the normalized intensity of the FLAG band for each condition to all other conditions. No pair-wise comparisons were significantly different. HEAT, Huntington, Elongation factor 3, A subunit of protein phosphatase 2A, and Tor1 kinase; Kapβ2, Karyopherin-β2.

not be stable or may be expressed poorly. However, low expression did not appear to be an issue. Using an antibody that recognizes an epitope in H8 of Kapβ2, we found that H1-H10, H1-H13, H8-E, and H8-H16 were all expressed in yeast, although H8-H16 was expressed at lower levels (Fig. 2*B*). We were unable to detect H1-H4, H9-E, and H12-E with this antibody (Fig. 2*B*). Thus, to detect the other Kapβ2 truncations that lack H8, we appended a C-terminal FLAG tag to each construct to enable detection *via* immunoblot using anti-FLAG antibodies.

We next tested the toxicity of the FLAG-tagged Kapβ2 truncations in the absence of FUS expression. Generally, the Kapβ2-FLAG constructs were not toxic, although Kapβ2-FLAG and H8-E-FLAG were very slightly toxic, whereas H1-H10-FLAG was toxic (Fig. S1*E*). As with untagged Kapβ2 constructs, only FL Kapβ2-FLAG and H8-E-FLAG mitigated FUS toxicity in yeast without affecting FUS expression (Fig. 2, *C* and *D*). All other Kapβ2 truncations were ineffective (Fig. 2*C*). The activity of FL Kapβ2-FLAG was reduced compared to untagged FL Kapβ2 despite similar expression levels, but Kapβ2-FLAG could still mitigate FUS toxicity (Figs. 2*C* and S1*F*). Importantly, H8-E-FLAG strongly reduced FUS toxicity (Fig. 2*C*).

Western blots revealed that there was some variation in Kapβ2-FLAG construct expression (Fig. 2, *D* and *E*). For example, H12-E-FLAG was expressed at consistently lower levels than FL Kapβ2-FLAG (Fig. 2, *D* and *E*). H9-E-FLAG was also expressed at lower levels than FL Kapβ2-FLAG (Fig. 2, *D* and *E*). Due to variability between samples, however, these differences were not statistically significant (Fig. 2*E*). Hence, it remains somewhat uncertain whether the reduced expression of H12-E-FLAG or H9-E-FLAG contributes to limited mitigation of FUS toxicity. Nevertheless, each construct was detectable *via* Western blot when probed with the anti-FLAG antibody. Thus, all the Kapβ2 constructs were expressed, and H1-H4-FLAG, H1-10-FLAG, H1-H13-FLAG, H8-E-FLAG, and H8-H16-FLAG were expressed at similar or increased levels compared to FL Kapβ2-FLAG (Fig. 2, *D* and *E*). However, only FL Kapβ2 and H8-E were able to mitigate FUS toxicity. Our findings suggest that when any single set of epitope contacts is lost, Kapβ2 is no longer able to mitigate FUS toxicity in yeast.

Truncated Kapβ2 proteins promote FUS solubility and nuclear localization in yeast

We next determined whether truncated Kapβ2 variants could suppress FUS aggregation and promote nuclear FUS localization in yeast. We did not explore the H1-H10 construct further due to its toxicity (Fig. S1, *A* and *E*). Yeast cells expressing FUS-GFP form cytoplasmic aggregates (92–94, 99, 103). Previously, we have found that potentiated variants of the Hsp104 disaggregase can dissolve these FUS aggregates without localizing FUS to the nucleus (94, 97–99, 103). By contrast, FL Kapβ2 suppresses FUS aggregation in yeast and localizes FUS to the nucleus (Fig. 3, *A*–*C*) (16). For the Kapβ2 truncations expressed here, the ratio of FUS-GFP expression to the loading control, α-tubulin, is relatively constant (Fig. 3*D*). Thus, the chaperone activity observed is attributable to Kapβ2 activity and not degradation or reduced expression of FUS.

Among the truncated Kapβ2 proteins, we observed a range of phenotypes. H1-H4-FLAG, H8-H16, and H12-E-FLAG were unable to prevent FUS aggregation or localize FUS to the nucleus (Fig. 3, *A*–*C*). By contrast, H1-H13 and H9-E-FLAG exhibited an intermediate phenotype. These truncations were unable to localize FUS to the nucleus but did reduce the percentage of cells with cytoplasmic FUS foci (Fig. 3, *A*–*C*). This phenotype is distinct from yeast expressing FUS-GFP and Kapβ2$^{W460A:W730A}$, which neither dissolves cytoplasmic FUS aggregates nor promotes FUS nuclear localization (16). Western blot confirmed that the lower level of cytoplasmic FUS foci is not due to the increased expression of the Kapβ2 truncation, as H9-E-FLAG is expressed at lower levels than Kapβ2-FLAG (Fig. 3*D*). Thus, a decrease in cytoplasmic FUS foci without increased nuclear localization suggests that, in yeast, H1-H13 and H9-E-FLAG may partially inhibit FUS aggregation in the cytoplasm but are inactive as NIRs.

The partial inhibition of FUS aggregation by H1-H13 and H9-E-FLAG was insufficient to mitigate FUS toxicity (Fig. 2, *A* and *C*). FUS must aggregate in the cytoplasm *and* bind RNA to confer toxicity in yeast (93). Kapβ2 can cause FUS to eject bound RNA (17, 19). Hence, it may be that truncated Kapβ2 proteins have reduced ability to eject bound RNA from FUS. Thus, FUS would continue to sequester important RNA transcripts and confer toxicity in yeast. Alternatively, the limited effect on FUS aggregation by H1-H13 or H9-E-FLAG may simply be insufficient to reduce FUS toxicity.

Consistent with the ability to mitigate FUS toxicity as well as Kapβ2, H8-E robustly suppresses FUS aggregation and localizes FUS to nucleus (Fig. 3, *A*–*C*). This finding suggests that all the information needed to chaperone FUS and transport it to the nucleus is encoded in HEAT repeats 8 to 20.

A C-terminal fragment of Kapβ2, H8-E, robustly prevents FUS fibrillization in vitro

For a more direct assessment of the chaperone activity of truncated Kapβ2 variants, we purified recombinant Kapβ2, Kapβ2$^{W460A:W730A}$, various Kapβ2 truncations (Fig. S2*A*), and FUS to measure chaperone activity *in vitro*. FUS is intrinsically aggregation-prone, and thus to maintain solubility during purification, FUS was purified with an N-terminal GST-tag (93). The bulky nature of GST precludes the PrLDs of FUS molecules from interacting with each other, thus preventing fibrillization (93). Additionally, there is a linker between the GST-tag and FUS which contains a TEV protease cleavage site. Thus, TEV protease can be utilized to initiate FUS fibrillization, which can be tracked *via* turbidity measurements (16, 93). Upon cleavage of GST-FUS with TEV protease, liberated FUS rapidly assembles into fibrils, which can be detected by an increase in turbidity (absorbance at 395 nm) (16, 37, 38, 93). The FUS fibrils that form *in vitro* resemble the fibrils observed in postmortem tissue and are toxic to neurons in culture and thus represent a biologically relevant structure to study (62, 93).

Purification of Kapβ2, Kapβ2$^{W460A:W730A}$, H1-H13, and H8-E was routine (Fig. S2*A*). However, we noticed that the expression, yield, and purity of H9-E were lower than for H1-H13 or H8-E (Fig. S2*A*). Previous work has indicated that HEAT-repeat proteins can be sensitive to truncation (104, 105). In the structural studies of other HEAT-repeat proteins, some truncations are stable, whereas others are aggregation-prone (104, 105). Indeed, purified H8-H16, which is inactive in yeast (Figs. 2, *A* and *C* and 3, *A*–*C*), is even more unstable

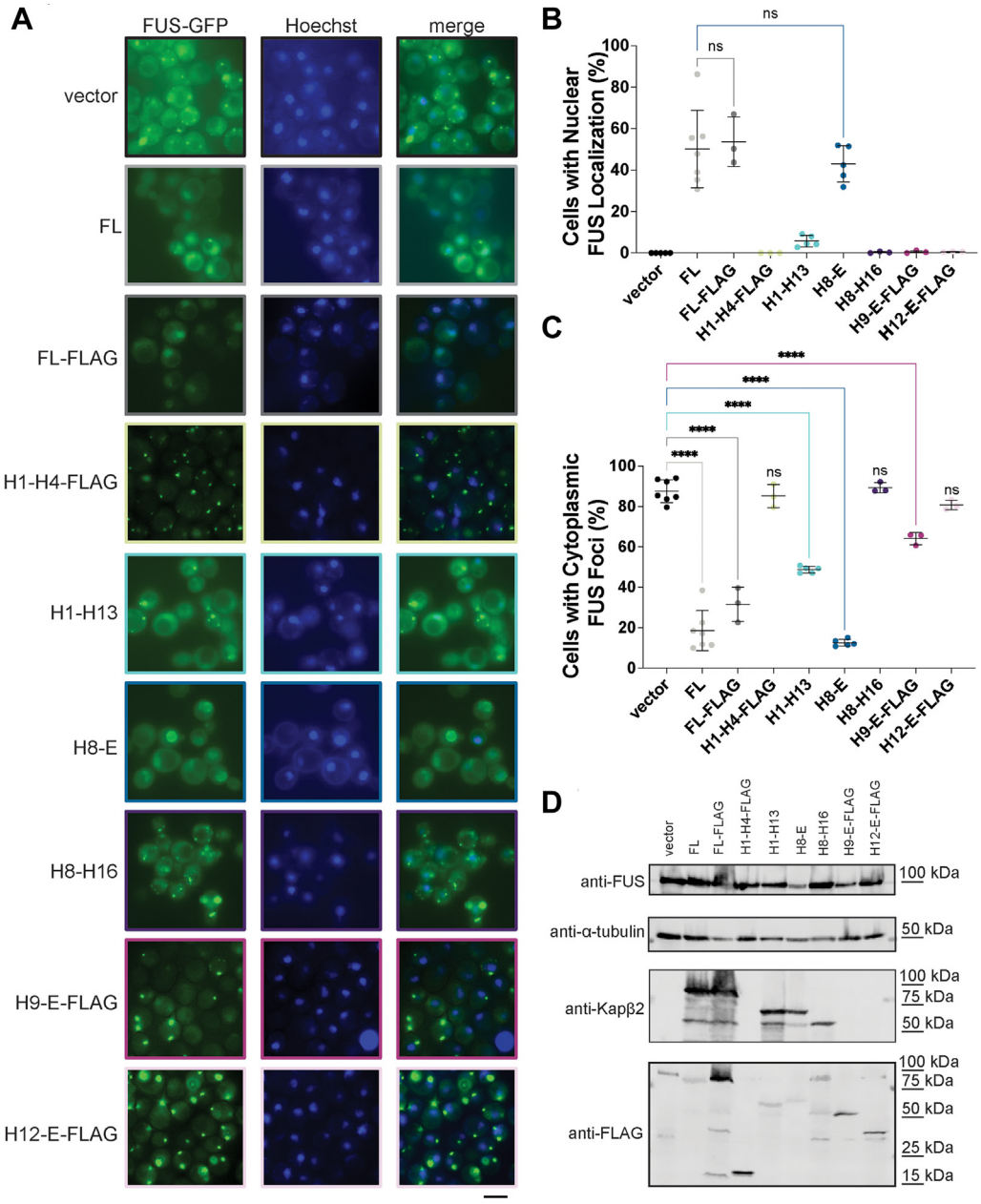

Figure 3. Kapβ2 and H8-E resolve cytoplasmic FUS foci and promote nuclear localization of FUS in yeast. *A*, Δ*hsp104* yeast with integrated galactose-inducible FUS-GFP were transformed with the indicated galactose-inducible Kapβ2 truncation and grown in galactose-containing media for 5 h. At this time, fluorescence microscopy reveals that yeast without Kapβ2 harbor cytoplasmic FUS foci. In contrast, cells expressing FL Kapβ2 (untagged or with a C-terminal FLAG tag) have a low proportion of cells with cytoplasmic FUS foci and a large proportion of cells with nuclear FUS localization. Similar results are observed with H8-E. Expression of H1-H13 or H9-E-FLAG can reduce the proportion of cells with cytoplasmic FUS foci without restoring nuclear FUS localization. H1-H4-FLAG, H8-H16, and H12-E-FLAG are unable to decrease the proportion of cells with cytoplasmic FUS foci or increase the proportion of cells with nuclear FUS localization. Scale bar represents 5 μm. *B*, quantification of the percentage of cells with nuclear FUS localization for each condition. Points represent independent transformations, and at least 100 cells were counted per transformation. Values represent means ± SD, n = 3 to 7. For cells with nuclear FUS localization, an ordinary one-way ANOVA with Dunnett's multiple comparisons test was used to compare the percentage of cells with nuclear localization in each condition to cells expressing FL Kapβ2. *C*, quantification of the percentage of cells with cytoplasmic FUS foci. Points represent independent transformations, and at least 100 cells were counted per transformation. Values represent means ± SD, n = 3 to 7. An ordinary one-way ANOVA with Dunnett's multiple comparisons test was used to compare the percentage of cells with cytoplasmic FUS foci in each condition to the vector control; ****$p < 0.0001$. *D*, Western blot of FUS-GFP yeast transformed with vector alone, FL Kapβ2, or the indicated Kapβ2 truncation. Probing with anti-FUS and anti–alpha-tubulin shows similar levels of protein expression across samples. Kapβ2 truncation expression, however, does vary, with H9-E-FLAG and H12-E-FLAG expressed at low levels relative to FL Kapβ2-FLAG. FL, full-length; Kapβ2, Karyopherin-β2.

than H9-E *in vitro* and becomes insoluble upon cleavage of its His-SUMO solubility tag by ubiquitin-like-specific protease 1 (Ulp1). This instability of H8-H16 suggests that C-terminal H17-H20 are important for protein stability in the absence of H1-H7. To circumvent this issue, we purified His-SUMO–tagged H8-H16 without cleavage (Fig. S2*A*). FL Kapβ2 chaperone activity is nearly identical between the Ulp1-cleaved and uncleaved constructs (Fig. S2, *B* and *C*), indicating there is no effect of the His-SUMO tag itself on the chaperone activity for FL Kapβ2. Thus, we do not anticipate that the His-

SUMO tag would affect activity of the H8-H16 construct. However, in the context of H8-H16, the His-SUMO tag is closer to the FUS-binding site, which might potentially have some effect on activity. Nonetheless, H8-H16 displays no activity against FUS in yeast (Figs. 2, *A* and *C* and 3, *A*–*C*), indicating that this construct may be defective.

Next, we assessed the extent of FUS fibrillization in the presence of increasing concentrations of each Kapβ2 construct (Figs. 4, *A*–*F* and S2, *D* and *E*). FL Kapβ2 suppresses FUS fibrillization at sub-stoichiometric levels (Figs. 4*A* and S2*E*) (16). By contrast, Kapβ2$^{W460A:W730A}$ does not effectively prevent FUS fibrillization, even at over 3-fold excess (Fig. S2, *D* and *E*). Likewise, purified His-SUMO-H8-H16 and H9-E were unable to effectively prevent FUS fibrillization (Figs. 4, *E* and *F* and S2*E*). In agreement with the reduction in cytoplasmic FUS-GFP foci in yeast expressing H1-H13, H1-H13 can partially inhibit FUS fibrillization *in vitro*, but only at very high levels (Figs. 4*B* and S2*E*). Indeed, at the highest concentration tested, H1-H13 reduces FUS fibrillization to only ∼40% (Figs. 4*B* and S2*E*). In line with the suppression of FUS aggregation and toxicity observed in yeast, H8-E robustly prevents FUS fibrillization *in vitro* (Figs. 4*C* and S2*E*). Calculating the half maximal inhibitory concentration (IC_{50}) of each construct for the prevention of FUS fibrillization reveals that H8-E can prevent FUS fibrillization as effectively as FL Kapβ2 (Fig. 4*D*). Our findings suggest that the entire FUS-binding region of Kapβ2 is required to enable maximal inhibition of FUS fibrillization *in vitro*.

H8-E reverses FUS fibrillization in vitro *nearly as effectively as Kapβ2*

In addition to preventing the fibrillization of its cargo, Kapβ2 can also reverse the formation of preformed fibrils (16). However, more Kapβ2 is required to reverse FUS fibrillization

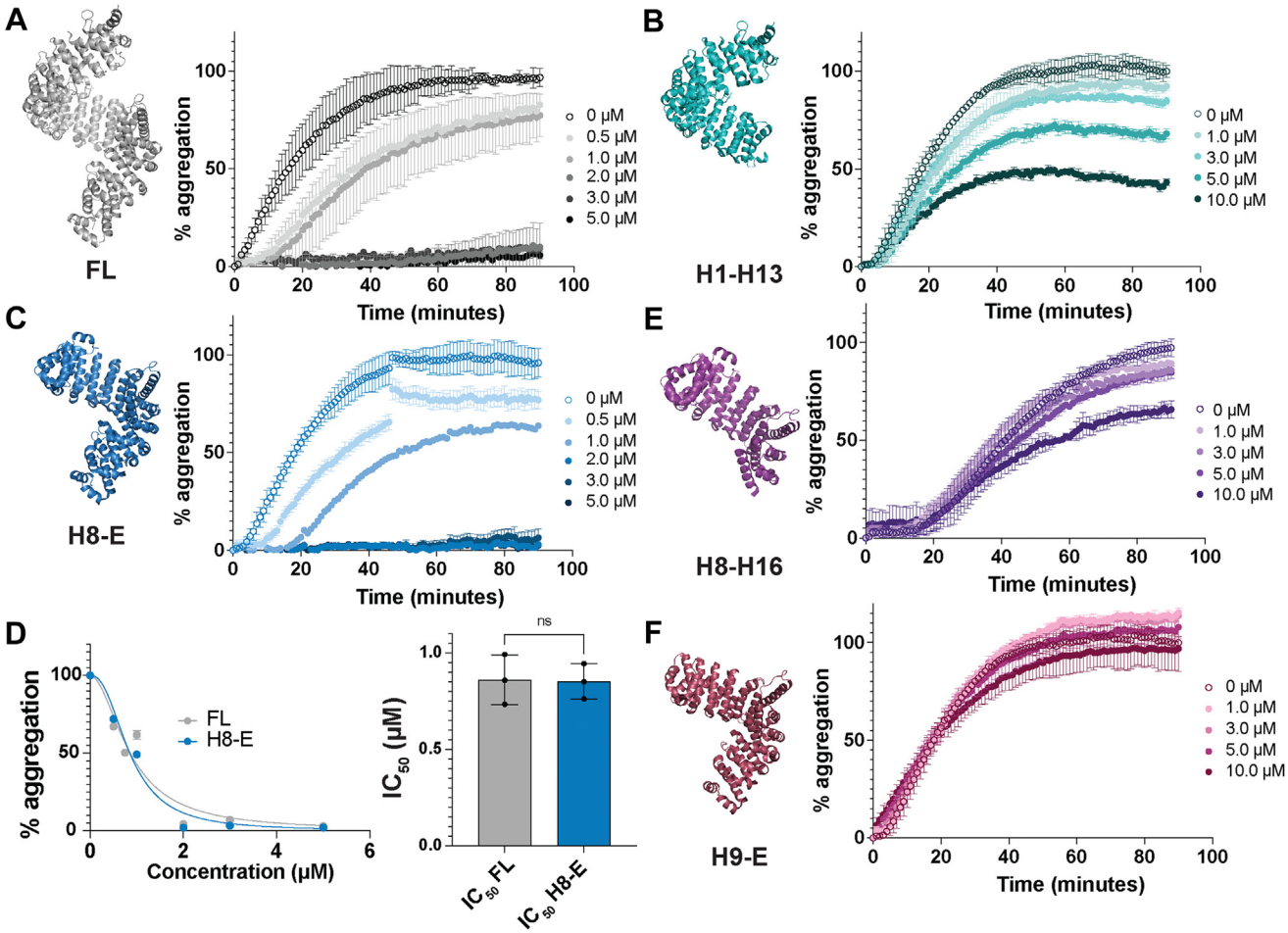

Figure 4. Kapβ2 and H8-E robustly suppress FUS fibrillization. To measure the ability of Kapβ2 constructs to prevent FUS fibrillization, we incubated 3 μM FUS with 1 μg TEV protease and the indicated concentration of Kapβ2 and monitored turbidity at 395 nm. Increased turbidity indicates FUS self-assembly into fibrils and each curve represents the mean of 2 to 4 trials ± SD. For each experiment, the maximal value of FUS turbidity in the absence of Kapβ2 was set to 100, and all data for that trial were normalized to that value. *A*–*C*, kinetics of FUS fibrillization in the presence of increasing concentrations of Kapβ2 (*A*), H1-H13 (*B*), or H8-E (*C*). FL Kapβ2 strongly suppresses FUS fibrillization. H1-H13 modestly inhibits FUS fibrillization, but only at stoichiometric excess. H8-E strongly suppresses FUS fibrillization. *D*, to compare the ability of FL Kapβ2 and H8-E to suppress FUS fibrillization, the area under the curve produced at each concentration was used to construct a curve of aggregation *versus* concentration (*left*). Comparing the half maximal inhibitory concentration (IC_{50}) reveals that the ability of H8-E to prevent FUS fibrillization is very similar to FL Kapβ2. IC_{50} values were derived from a nonlinear curve fit with normalized responses and a variable slope. Each calculated IC_{50} value is plotted with its 95% confidence interval. An unpaired *t* test was used to compare IC_{50} values. *E* and *F*, kinetics of FUS fibrillization in the presence of increasing concentrations of His-SUMO-H8-H16 (*E*) or H9-E (*F*). High concentrations of His-SUMO-H8-H16 slightly inhibit FUS fibrillization. H9-E is unable to prevent FUS fibrillization even in excess. The structures presented here are based on PDB: 2QMR. FL, full-length; Kapβ2, Karyopherin-β2.

than to prevent fibrillization (16). Thus, focusing on the truncations that had the most significant effect on preventing FUS fibrillization, H1-H13 and H8-E, we next determined whether truncated variants of Kapβ2 could disaggregate preformed FUS fibrils. For these experiments, FUS fibrillization was initiated by the addition of TEV protease in the absence of Kapβ2. After 1 h of FUS fibrillization when abundant FUS fibrils are present (93), Kapβ2 was added, and turbidity was monitored.

As expected, FL Kapβ2 rapidly disaggregates FUS fibrils (Fig. 5*A*) (16, 106). FL Kapβ2 completely disaggregates FUS fibrils after 10 min at a ratio of ∼3:1 Kapβ2 to FUS (Fig. 5*A*). By contrast, Kapβ2$^{W460A:W730A}$ was unable to disaggregate preformed FUS fibrils (Fig. S3, *A* and *B*). H1-H13 was also ineffective at disaggregating FUS fibrils but displayed some activity (Figs. 5*B* and S3*B*). At the highest concentration tested, H1-H13 was able to reduce turbidity by ∼50% after 80 min (Fig. 5*B*). Additionally, the shape of the FUS disaggregation curve for H1-H13 is distinct from what is observed with FL Kapβ2 (Fig. 5, *A* and *B*). For FL Kapβ2, FUS disaggregation begins immediately after addition and decreases rapidly (Fig. 5*A*). By contrast, addition of H1-H13 initially causes a sharp decline in FUS turbidity, followed by apparent re-aggregation and subsequent slow disaggregation (Fig. 5*B*). These data indicate that H1-H13 has limited ability to effectively disaggregate FUS.

Importantly, H8-E is a robust chaperone that readily disaggregates preformed FUS fibrils (Figs. 5*C* and S3*B*). However, H8-E requires a longer time to completely disaggregate FUS, as complete disaggregation is not achieved until ∼20 min (Fig. 5*C*), whereas FL Kapβ2 only requires ∼10 min (Fig. 5*A*). Moreover, the half maximal effective concentration (EC_{50}) of H8-E required to disaggregate FUS is ∼2-fold higher than for FL Kapβ2 (Fig. 5*D*). Thus, H8-E can disaggregate FUS fibrils at sub-stoichiometric levels, but it is unable to disaggregate FUS fibrils as effectively as FL Kapβ2. Our findings suggest that the N-terminal H1-H7 region of Kapβ2 is more critical for optimal reversal of FUS fibrillization than for inhibition of FUS fibrillization. Indeed, the N-terminal H1-H7 region of Kapβ2 appears to enable optimal disaggregation activity.

H8-E dissolves preformed FUS liquid condensates

FUS undergoes liquid-liquid phase separation to spontaneously form dynamic condensates, which are important for FUS functionality, but may precede pathological aggregation and thus require vigilant chaperoning (54, 61, 65, 70, 107, 108). *In vitro*, FUS readily forms liquid condensates in the presence of Cy3-labeled poly(U) RNA (20). Thus, we next tested if the Kapβ2 truncations that effectively work on solid-like FUS fibrils would also dissolve heterotypic liquid-liquid phase-separated FUS:RNA condensates. FL Kapβ2 can dissolve preformed FUS:RNA condensates, resolubilizing both the RNA (Fig. 6*A*) and FUS (Fig. 6*B*) components of these condensates (20, 21, 24). FL Kapβ2 reduces the number of FUS:RNA droplets (Fig. 6*C*), the total area of these structures (Fig. 6*D*),

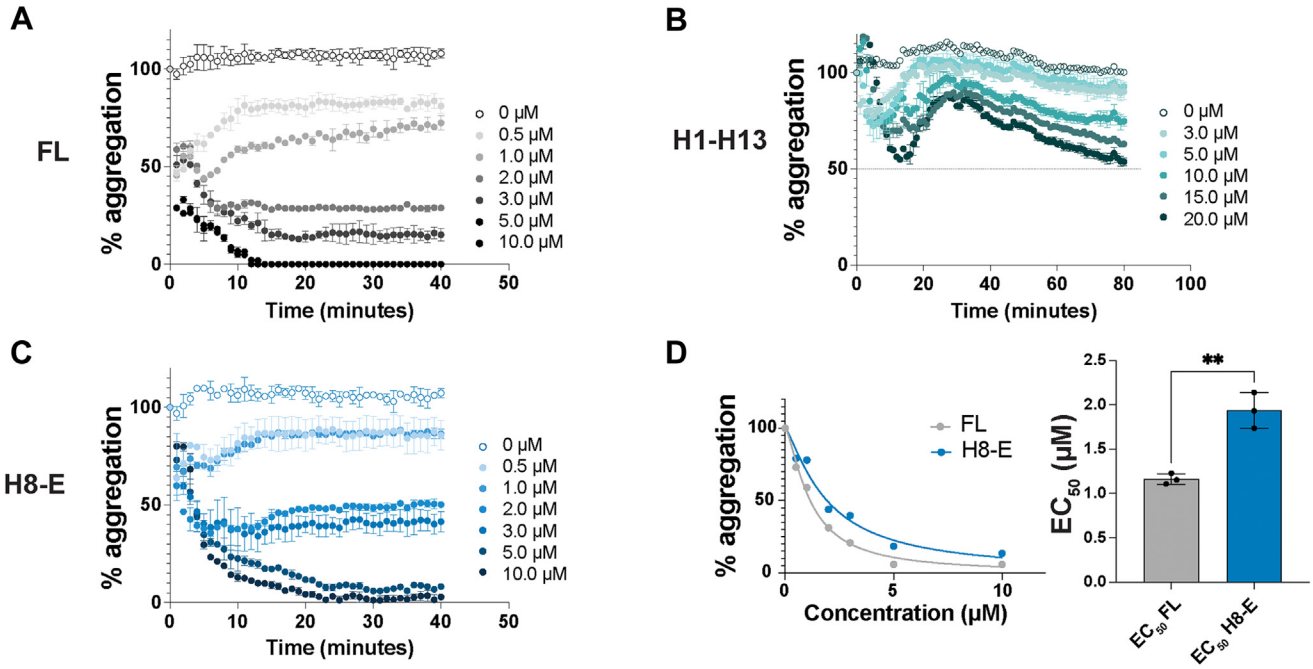

Figure 5. Kapβ2 and H8-E robustly disaggregate FUS fibrils. To measure the ability of Kapβ2 constructs to disaggregate FUS fibrils, we incubated 3 μM FUS with 1 μg TEV protease and monitored turbidity at 395 nm. After 1 h of fibrillization, the indicated amount of Kapβ2 was added and turbidity was continually measured. Each curve represents the mean of 2 to 3 trials ± SD. For each condition, the value of FUS turbidity immediately prior to adding Kapβ2 was set to 100 and all subsequent readings were normalized to that value. *A–C*, kinetics of FUS disaggregation by FL Kapβ2 (*A*), H1-H13 (*B*), or H8-E (*C*). FL Kapβ2 and H8-E rapidly disaggregate FUS. H1-H13 can partially reverse FUS fibrillization, but only to ∼50% and over an extended period. *D*, to compare the activity of FL Kapβ2 and H8-E, the area under the curve produced at each concentration was used to construct a curve of aggregation *versus* concentration (*left*). Half maximal effective concentration (EC_{50}) values were derived from a nonlinear curve fit with normalized responses and a variable slope. Each calculated EC_{50} value is plotted with its 95% confidence interval. Comparing the EC_{50} reveals that the ability for H8-E to reverse FUS fibrillization is somewhat impaired relative to Kapβ2. An unpaired *t* test was used to compare EC_{50} values. $^{**}p < 0.005$. FL, full-length; Kapβ2, Karyopherin-β2.

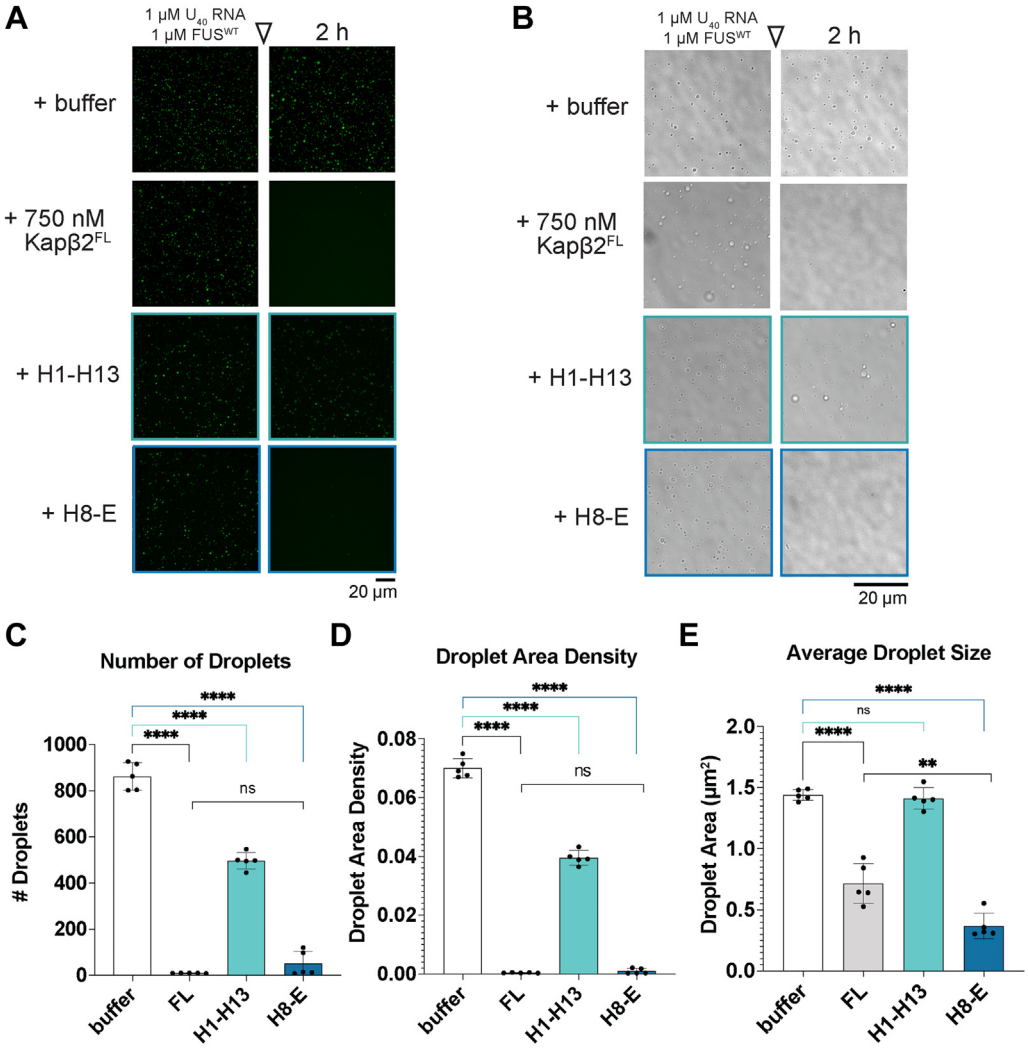

Figure 6. Kapβ2 and H8-E disperse heterotypic FUS:RNA condensates. *A–E*, to assess the ability of Kapβ2 and truncation constructs to disperse FUS:RNA droplets, we mixed 1 μM Cy3-labeled U_{40} RNA with 1 μM FUS, which form liquid-like droplets after 4 h. Taking images using fluorescence microscopy (*A*) or brightfield microscopy (*B*) 2 h after the addition of buffer or the indicated Kapβ2 construct demonstrates that FUS:RNA droplets are unaffected by the addition of buffer (scale bar represents 20 μm). By contrast, FL Kapβ2 (0.75 μM) effectively disperses FUS:RNA droplets, reducing them in number (*C*), overall area of the coverslip occupied by condensates (*D*), and the average size of each droplet (*E*). H1-H13 can also reduce the number and total area of FUS:RNA droplets, but is not as effective as FL Kapβ2, and does not decrease individual droplet size. However, an equal concentration of H8-E can reduce the number and area of FUS:RNA droplets to a similar extent as FL Kapβ2. Data points in (*C–E*) represent individual images, and bars represent means ± SD, n = 5. An ordinary one-way ANOVA with Dunnett's multiple comparisons test was used to compare the value for each condition to that of buffer alone. ****$p <$ 0.0001. Additionally, an unpaired *t* test was used to compare FL and H8-E. **$p < 0.004$. FL, full-length; Kapβ2, Karyopherin-β2.

and the average size of the individual remaining droplets (Fig. 6*E*). H1-H13 also significantly reduced the number and total area of FUS:RNA droplets after addition, but only by ∼44% as opposed to the near 100% reduction observed for FL Kapβ2 (Fig. 6, *A–D*). However, the average droplet size was unchanged by H1-H13 (Fig. 6*E*). These data are consistent with the limited ability of H1-H13 to antagonize FUS fibrillization (Fig. 5*B*).

Like FL Kapβ2, H8-E significantly reduced the number, total area, and average size of FUS:RNA droplets, performing as effectively as Kapβ2 (Fig. 6, *A–E*). The total number and area of droplets resulting after treatment with Kapβ2 and H8-E are similar (Fig. 6, *C* and *D*), but the average size of the remaining droplets is lower for H8-E (Fig. 6*E*). Thus, the few droplets that remain in the presence of H8-E are even smaller than those that remain with Kapβ2. Our findings suggest that H8-E effectively dissolves FUS liquids, and in this context, the N-terminal H1-H7 of Kapβ2 is less important. Hence, it appears that the N-terminal H1-H7 region of Kapβ2 is critical for optimal disaggregation of solid FUS condensates but not liquid FUS condensates.

Truncated Kapβ2 proteins reduce cytoplasmic foci and restore nuclear localization in human cells

Finally, we explored how Kapβ2 and truncation variants might affect FUS condensation and localization in human cells. The overexpression of GFP-FUS plus mCherry (negative control) in Henrietta Lacks' (HeLa) cells induces the formation of cytoplasmic FUS foci (Fig. 7, *A* and *B*). Coexpression of

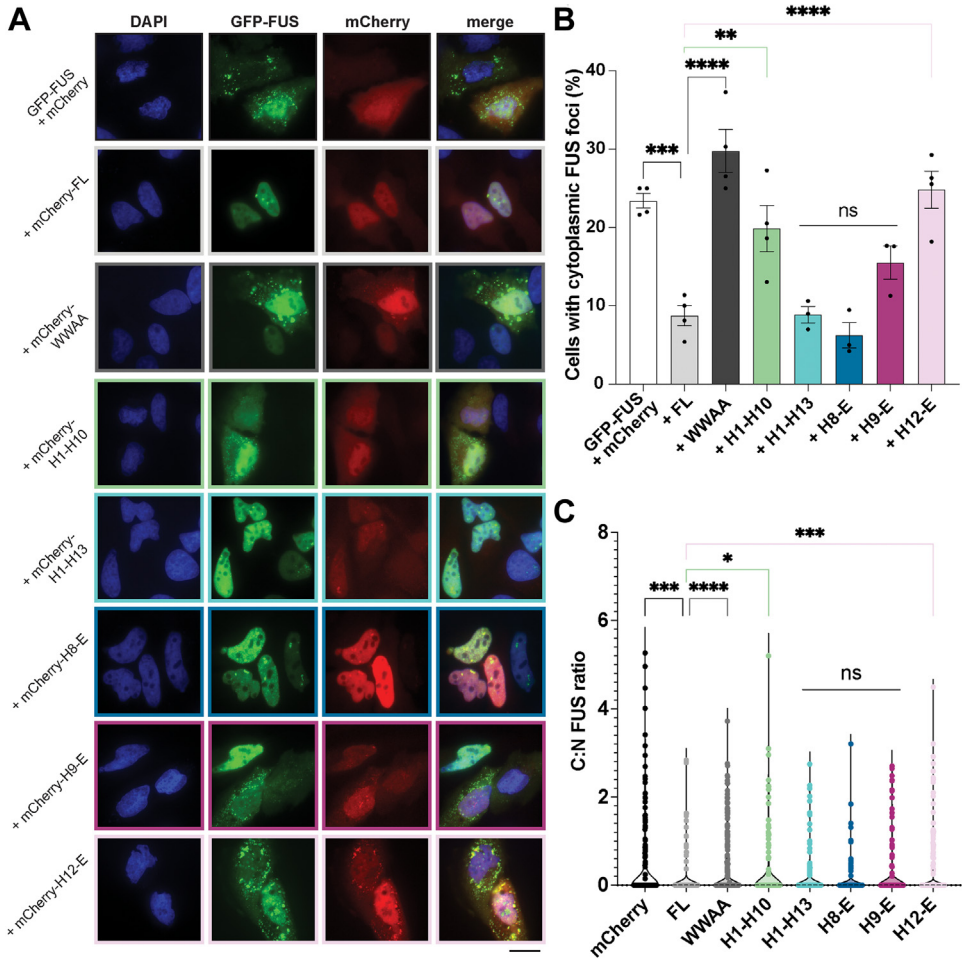

Figure 7. Kapβ2 and H8-E prevent the formation of cytoplasmic FUS foci and promote FUS nuclear localization in human cells. *A*, in HeLa cells, expression of GFP-FUS with mCherry alone results in ∼25% of cells with cytoplasmic FUS puncta. When mCherry-FL-Kapβ2 is coexpressed with GFP-FUS, FUS is largely localized to the nucleus, with many fewer cells exhibiting cytoplasmic mislocalization. Furthermore, expression of H1-H13, H8-E, or H9-E also reduces the proportion of cells with cytoplasmic FUS foci. In contrast, cytoplasmic foci persist when H1-H10 and H12-E are expressed. These results suggest that in human cells where endogenous FL Kapβ2 is present, H1-H13 and H9-E can complement the endogenous chaperone machinery to antagonize FUS condensation and promote nuclear import. Scale bar represents 20 μm. *B*, quantification of the percentage of cells with cytoplasmic FUS foci indicates that the activity of each H1-H13, H8-E, and H9-E each is not statistically different from FL Kapβ2. Each point represents independent transfections. At least 100 cells were counted over three separate trials; data points represent individual transfections and bars show means ± SEM, n = 3 to 4. An ordinary one-way ANOVA with Dunnett's multiple comparisons test was used to compare the percentage of cells with foci in each condition to cells expressing FL Kapβ2. $^{**}p < 0.005$; $^{***}p < 0.0005$; $^{****}p < 0.0001$. *C*, quantifying the ratio of GFP signal coming from the cytoplasm and the nucleus shows that H1-H13, H8-E, and H9-E promote nuclear FUS localization to a level that is similar to that of FL Kapβ2. H1-H10 and H12-E, however, are not as effective. Each point represents a single cell, n > 150 for each condition. A Kruskal-Wallis test with Dunn's multiple comparisons test was used to compare the nuclear GFP-FUS signal in each condition to cells expressing FL Kapβ2. $^{*}p < 0.05$; $^{***}p < 0.0009$; $^{****}p < 0.0001$. FL, full-length; Kapβ2, Karyopherin-β2.

mCherry-FL-Kapβ2 significantly reduced the formation of cytoplasmic FUS foci (Fig. 7, *A* and *B*). In contrast, expression of mCherry-Kapβ2$^{W460A:W730A}$ exacerbates formation of cytoplasmic FUS foci (Fig. 7, *A* and *B*). Of the truncation constructs, neither mCherry-H1-H10 nor mCherry-H12-E reduced the percentage of cells with cytoplasmic FUS foci (Fig. 7, *A* and *B*). Coexpression of mCherry-H8-E or mCherry-H1-H13 reduced the percentage of cells with cytoplasmic FUS foci to a similar extent as Kapβ2 (Fig. 7, *A* and *B*). Unexpectedly, H9-E also reduced the formation of cytoplasmic FUS foci (Fig. 7, *A* and *B*). mCherry-H8-H16 was barely visible *via* microscopy, and was not detected *via* Western blot, and thus was not analyzed further (Fig. S4). Moreover, there was variable expression of each expressed Kapβ2 construct (Fig. S4). FL Kapβ2, Kapβ2$^{W460A:W730A}$, H1-H10, and H12-E were each robustly expressed, whereas H1-H13, H8-E, and H9-E were expressed at lower levels (Fig. S4). However, despite the low expression, H1-H13, H8-E, and H9-E mitigated formation of cytoplasmic FUS foci (Fig. 7, *A* and *B*). Moreover, GFP-FUS was similarly expressed across all cells relative to the α-tubulin loading control (Fig. S4). Thus, differences in FUS expression do not contribute to the reduced formation of cytoplasmic FUS foci.

We next assessed the ratio GFP-FUS signal coming from the cytoplasm and the nucleus to measure how proficient each construct is as an NIR (Fig. 7*C*). As expected, expression of Kapβ2 promoted nuclear localization of GFP-FUS significantly more than the expression of mCherry alone (Fig. 7*C*). Conversely, Kapβ2$^{W460A:W730A}$ did not increase the fraction of GFP-FUS in the nucleus (Fig. 7*C*). Similar to their inability to

reduce cytoplasmic FUS foci, H1-H10 and H12-E were also unable to restore nuclear localization of FUS as well as Kapβ2 (Fig. 7*C*). By contrast, H8-E promoted nuclear localization of GFP-FUS as effectively as Kapβ2.

Curiously, H1-H13 and H9-E also promoted nuclear localization of GFP-FUS as well as Kapβ2 (Fig. 7*C*). This finding was unexpected, as in yeast, these truncations could only reduce cytoplasmic foci (Fig. 3, *B* and *C*). However, one important difference between the yeast and HeLa cell models is that yeast lack Kapβ2. Indeed, yeast utilize Kap104 to perform Kapβ2-like transport activity (12, 13, 109). Although Kap104 can weakly bind to the PY-NLS of FUS, Kap104 preferentially binds basic PY-NLS sequences, whereas FUS harbors a hydrophobic PY-NLS (13, 14). Indeed, any *in vitro*–binding capacity Kap104 may retain for FUS is insufficient for chaperone activity in yeast when FUS is overexpressed (Fig. 2) (16, 92, 93). By contrast, HeLa cells harbor endogenous Kapβ2. Thus, even low levels of truncated Kapβ2 variants may be able to collaborate with endogenous Kapβ2 to effectively reduce the formation of cytoplasmic FUS foci and promote nuclear localization of FUS. Indeed, in HeLa cells, there is a noticeable increase in the cytoplasmic mCherry signal for H1-H10, H1-H13, H9-E, and H12-E, suggesting these proteins may be defective for nuclear import (Fig. 7*A*). The increased levels of cytoplasmic truncated Kapβ2 suggest that all truncations except H8-E are deficient in their ability to traverse in and out of the nucleus but retain some inherent chaperone activity in the cytoplasm that cooperates with endogenous Kapβ2. In yeast, this cytoplasmic chaperone activity manifests as a diffuse cytoplasmic FUS signal as Kap104 does not import FUS into the nucleus (13, 92, 93). In HeLa cells, cytoplasmic chaperone activity may help liberate FUS from cytoplasmic foci, making it available to the endogenous transport-competent Kapβ2.

Our findings suggest that H8-E is a robust chaperone, performing as well as FL Kapβ2 in several contexts, including (1) preventing FUS toxicity and promoting FUS nuclear localization in yeast, (2) preventing FUS fibril formation *in vitro*, (3) dispersing FUS liquid condensates *in vitro*, and (4) reducing cytoplasmic FUS foci and restoring nuclear localization of FUS in human cells. Our data demonstrate that the N-terminal H1-H7 region of Kapβ2 is not required for significant chaperone functionality. Nonetheless, the N-terminal H1-H7 region enables optimal disaggregation of FUS fibrils, indicating a functional role in disaggregation. Our findings definitively map the molecular chaperone and nuclear-import activities of Kapβ2 to H8-H20.

Discussion

Kapβ2 is an NIR that also demonstrates specific chaperone activity against its cargo *in vitro*, in yeast, in human cells, and in fly models (16). The structure and localization of Kapβ2 in cargo-bound and unbound states have been extensively characterized (7, 8, 12, 81, 83, 86). However, it has remained unclear precisely how the structure of Kapβ2 is directly related to its chaperone activity. Here, we designed truncated variants of Kapβ2 that eliminate its binding to specific epitopes of the FUS PY-NLS to determine which regions of Kapβ2 are most critical for chaperoning cargo and importing cargo into the nucleus.

In a yeast model system where the Kapβ2 cargo protein FUS is toxic (92–94), FL Kapβ2 mitigates FUS toxicity. H8-E, the only Kapβ2 truncation that includes all three PY-NLS epitope-binding regions, can also suppress FUS toxicity in this model. When GFP-tagged FUS is expressed in yeast, it forms abundant cytoplasmic aggregates and is depleted from the nucleus. Expression of FL Kapβ2 resolves these cytoplasmic aggregates and localizes FUS to the nucleus. In line with the results from yeast toxicity assays, H8-E also eliminates cytoplasmic FUS foci and promotes nuclear FUS localization. Indeed, H8-E was the only Kapβ2 truncation variant tested here to phenocopy Kapβ2 in yeast. None of the other Kapβ2 truncation constructs could mitigate FUS aggregation *and* toxicity.

Interestingly, truncations H1-H13 and H9-E, which did not mitigate FUS toxicity in yeast, displayed an intermediate phenotype where cytoplasmic FUS foci were partially dissolved without robust nuclear import. Previous work has established that dissolving cytoplasmic FUS aggregates with potentiated variants of the AAA+ disaggregase Hsp104 without promoting nuclear import can suppress FUS toxicity (94, 97, 99, 103, 110). However, the partial decrease in cytoplasmic FUS foci conferred by H1-H13 or H9-E is insufficient to suppress FUS toxicity. Thus, our data suggest that truncated variants of Kapβ2 that contain only a portion of the known PY-NLS–contacting residues have a diminished capability to antagonize cytoplasmic FUS aggregation, restore nuclear localization, and prevent cargo-related toxicity in yeast.

We also assessed the ability of truncated Kapβ2 proteins to directly chaperone FUS at the pure protein level. Kapβ2 potently prevents and reverses FUS fibrillization in this setting (16). H8-E, which counters FUS toxicity and aggregation in yeast as well as FL Kapβ2, also chaperones FUS *in vitro*, although its ability to disaggregate FUS fibrils is mildly impaired compared to that of FL Kapβ2. H1-H13, on the other hand, only chaperones FUS at very high concentrations and was unable to completely prevent or reverse FUS fibrillization. H8-H16 can weakly prevent FUS fibrillization, but its chaperone activity is substantially lower than even that of H1-H13. Surprisingly, although H9-E makes partial contact with the PY-epitope of the PY-NLS of FUS, the protein was inactive *in vitro*. However, the yield from the purification of H8-H16 and H9-E was low compared to H1-H13, H8-E, or Kapβ2, indicating that H8-H16 and H9-E may be less stable, which could affect chaperone activity. Nevertheless, these data indicate that HEAT repeat 8 plays a critical role for *in vitro* chaperone activity and that the entire FUS-PY-NLS–binding region of Kapβ2 enables chaperone activity. We also assessed the ability of Kapβ2 and truncated variants to dissolve FUS:RNA liquid condensates. In this context, H1-H13 has ∼44% FL Kapβ2 activity, whereas FL Kapβ2 and H8-E rapidly dissolve FUS:RNA liquid condensates, significantly reducing their number, total area, and average size.

Why is H8-E, which performs as well as Kapβ2 in all other respects, mildly deficient (*i.e.*, ∼2-fold increase in EC_{50}) in disaggregating preformed FUS fibrils? This finding suggests

that the N-terminal H1-H7 region contributes toward optimal disaggregation of FUS fibrils. We suggest that H1-H7 may make secondary contacts with the FUS PrLD after Kapβ2 has engaged the FUS PY-NLS, which help break the intermolecular contacts that hold FUS fibrils together (6, 16, 19). These contacts may be akin to interactions that NIRs make with FG-rich nucleoporins (Nups) during passage across the nuclear-pore complex (111–114). Indeed, the N-terminal HEAT repeats of a related NIR, Kapβ1, make contacts with FG-rich Nups (111). Moreover, a related nuclear-export factor, CRM1, may prevent FG-rich Nup condensation in the cytoplasm (115). Regardless, H8-E can still disaggregate FUS fibrils, albeit less efficiently than FL Kapβ2, indicating that residues beyond H1-H7 can also break contacts between FUS PrLDs that preserve fibril integrity.

A critical element in the structure of Kapβ2 is an extended acidic loop in H8. In the cytoplasm, where Ran is primarily in its GDP-bound state, the H8 loop is disordered and the Kapβ2 cargo-binding surface is available to interact with cargo (1, 7, 82, 86). When Kapβ2 is bound to Ran-GTP in the nucleus, the H8 loop repositions to occupy the internal cargo-binding surface of Kapβ2, displacing the loaded cargo (116). Thus, this extended loop is necessary for cargo unloading in the presence of Ran-GTP (83, 116). The extended loop is not, however, required for Kapβ2 disaggregation activity (16). Indeed, Kapβ2 with a truncated acidic loop (Kapβ2^{TL}, in which residues 341–362 are replaced by a 7-residue GGSGGSG linker) still acts as a chaperone *in vitro* to prevent and reverse FUS aggregation, and Kapβ2^{TL} prevents and reverses FUS recruitment to SGs in cells (16, 116). Thus, Kapβ2 chaperone activity can be separated from its role in nuclear import. Nonetheless, Kapβ2^{TL} would have limited ability to restore FUS to the nucleus and mitigate any loss of FUS nuclear function.

We also assessed the activity of Kapβ2 and truncated variants in human cells. Overexpression of GFP-FUS in HeLa cells results in the formation of cytoplasmic FUS foci. However, when mCherry-FL-Kapβ2 or -H8-E is coexpressed, GFP-FUS is transported into the nucleus and the proportion of cells with cytoplasmic GFP-FUS foci decreases. Coexpression of H1-H13 or H9-E also reduces the number of cells with cytoplasmic FUS foci, despite displaying reduced chaperone activity *in vitro*. Surprisingly, despite being unable to promote nuclear localization in yeast, H1-H13 and H9-E do promote nuclear localization of FUS in human cells. We therefore suggest that these Kapβ2 truncations may help endogenous Kapβ2 to antagonize formation of cytoplasmic FUS foci, allowing endogenous Kapβ2 to promote FUS nuclear localization.

Our findings establish that the entire FUS-binding region of Kapβ2 is required for effective chaperone and nuclear-import activity. Cargo recognition requires the eighth HEAT repeat, but the residues contained in this region are not sufficient for functionality. The importance of H8 here is consistent with previous work, as H8 contains residues that bind to the PY epitope of the PY-NLS, and this epitope contributes to the tight binding between Kapβ2 and cargo (1, 14). However, our work indicates that binding to non–PY-epitopes is also important and supports overall Kapβ2 function. Indeed, Kapβ2 relies on multiple low-affinity interactions to chaperone cargo (12, 19, 23, 117). Moreover, these data agree with genetic studies that have identified mutations in all three PY-NLS epitopes of FUS as causing ALS (14, 79, 118, 119). Similar mutations in the PY-NLS of hnRNPA1 and hnRNPA2 also cause degenerative disease (40, 41, 120, 121). We suggest that Kapβ2 chaperone activity is achieved by making an extensive network of both strong and weak interactions with cargo, displacing cargo:cargo interactions in favor of Kapβ2:cargo interactions. Mutating just two residues in Kapβ2 that engage cargo as in the Kapβ2$^{W460A:W730A}$ variant inactivates Kapβ2. Interestingly, H8-H16 and H9-E, each of which contains both Trp residues that are mutated to Ala in the Kapβ2$^{W460A:W730A}$ mutant, are inactive in yeast despite being well expressed. Thus, the specific interactions mediated by W460 and W730 are important but not sufficient for chaperone activity.

Can truncated Kapβ2 proteins be used to supplement endogenous levels of Kapβ2 function? In models of disease where Kapβ2 cargo proteins aggregate, increasing expression of Kapβ2 can restore cargo-protein functionality (16). Thus, boosting Kapβ2 activity is an intriguing therapeutic approach (6, 25–28, 122). Kapβ2 is a large protein, and thus delivering smaller portions of the protein may be a more tractable approach. Recent advances in AAV-mediated delivery of genetic material for exogenous protein production have made the prospect of gene therapy more realistic (123–125). However, AAVs are limited by their DNA-packaging capacity, which restricts the size of the protein they can express. Of the two AAV-based treatments approved by the United States Food and Drug Administration, the molecular weight of the largest protein to be expressed is ∼65 kDa (126, 127). Kapβ2 is ∼100 kDa, whereas H8-E is ∼70 kDa. Thus, it may be that with further technological improvements to AAV-based approaches, H8-E or even FL Kapβ2 could be delivered exogenously to treat diseases where nucleocytoplasmic trafficking of PY-NLS cargo is impaired, including ALS/FTD, MSP, oculopharyngeal muscular dystrophy, hereditary motor neuropathy, and related disorders (39–41, 128–131).

Experimental procedures

Key resources

Key resources are shown in Table 1.

Plasmids

Kapβ2 truncations were cloned in the following manner: H1-H4, H1-H10, and H1-H13 were created by inserting stop codons into a GST-TEV-Kapβ2 plasmid using the following primers with their respective reverse complements: 5′-GAC AGTGATGTTTTAGATCGTTAGTAGAACATCATG-3′; 5′-CAGCCGCCAGACACGTAGTAGAAGCCATTAATG-3′; and 5′-GGATTCCTTCCGTGATGAGAACCTGTGTATCA G-3′. H8-E, H9-E, and H12-E were cloned into a GST-TEV-Kapβ2 plasmid (1, 16) using the following primers with their respective reverse complements: 5′-CAGGGCGGATCCAA GGCTTTAGAAGCCTGTGAATTTTGG-3′; 5′-CAGGGCG

Table 1
Key resources

Reagent or resource	Source	Identifier
Antibodies		
Rabbit polyclonal anti-FUS	Bethyl	Cat# A300-302A; RRID: AB_309445
Mouse monoclonal anti-Flag (M2)	Sigma-Aldrich	Cat# F3165; RRID: AB_259529
Anti-Kapβ2 monoclonal antibody	Novus	Cat# NB600-1397
Rabbit monoclonal anti-alpha tubulin antibody	Abcam	Cat# ab184970
Rat monoclonal anti-tubulin antibody	Abcam	Cat# ab6160
Anti-GFP polyclonal antibody	Sigma-Aldrich	Cat# G1544
Anti-mCherry polyclonal antibody	Abcam	Cat# ab167453
Goat anti-rabbit secondary antibody	Li-cor	Cat# 926-68071; RRID: AB_10956166
Goat anti-mouse secondary antibody	Li-cor	Cat# 926-32210; RRID: AB_621842
Goat anti-rat secondary antibody	Li-cor	Cat# 926-32219; RRID: AB_1850025
Bacterial and Viral Strains		
Escherichia coli BL21-CodonPlus(DE3)-RIL	Agilent	Cat# 230245
E. coli XL 10-Gold cells	Agilent	Cat# 200314
One Shot TOP10 Chemically Competent *E. coli*	Invitrogen	Cat# C404010
Chemicals, Peptides, and Recombinant Proteins		
PfuUltra II Fusion HS DNA Polymerase	Agilent	Cat# 600672
DpnI	NEB	Cat# R0176S
Gateway BP Clonase II Enzyme Mix	Invitrogen	Cat# 11789013
Gateway LR Clonase II Enzyme Mix	Invitrogen	Cat# 11791019
NEBuilder HiFi DNA Assembly Master Mix	NEB	Cat# E2621S
Ni-NTA agarose	QIAGEN	Cat# 30230
Glutathione Sepharose 4 Fast Flow	GE Healthcare	Cat# GE17-5132-01
cOmplete, EDTA-free Protease Inhibitor Cocktail	Roche	Cat# 11873580001
Hoechst 33342 stain	Invitrogen	Cat# H3570
Lipofectamine 2000 Transfection Reagent	Invitrogen	Cat# 11668027
VECTASHIELD Antifade Mounting Medium with DAPI	Vector Laboratories	Cat# H-1200-10
DMEM, high glucose, pyruvate	Gibco	Cat# 11995065
Fetal bovine serum	Cytiva	Cat# SH30910.03
Penicillin-streptomycin	Gibco	Cat# 15140122
HisTrapFast Flow Crude	Cytiva	Cat# 17528601
Novex AcTEV Protease	Thermo Fisher Scientific	Cat# 12-575-015
Cy3 NHS Ester	Cytiva	Cat# PA13101
Critical Commercial Assays		
QuikChange Site-Directed Mutagenesis Kit	Agilent	Cat# 210518
Experimental Models: Organisms/Strains		
Saccharomyces cerevisiae: W303aΔhsp104 (MATa, can1-100, his3-11, 15, leu2-3, 112, trp1-1, ura3-1, ade2-1, hsp104::KanMX)	Ref. (134)	A3224
S. cerevisiae: W303aΔhsp104-pAG303GAL-FUS	Ref. (94)	N/A
S. cerevisiae: W303aΔhsp104-pAG303GAL-FUS-GFP	Ref. (94)	N/A
Experimental Models: Cell Lines		
Human: HeLa	ATCC	Cat# CCL-2; RRID:CVCL_0030
Recombinant DNA/RNA		
GST-TEV-FUS^{WT}	Ref. (93)	N/A
GST-TEV-Kapβ2	Ref. (16)	N/A
His-SUMO-Kapβ2 (FL and truncations)	This paper	N/A
pAG416Gal-Kapβ2 (FL and truncations)	This paper	N/A
mCherry2-C1	N/A	Addgene Cat# 54563
mCherry2-N1	N/A	Addgene Cat# 54517
pEGFP-C1-FLAG	Ref. (135)	GenBank U55763.1
mCherry2-Kapβ2 (FL and truncations)	This paper	N/A
pEGFP-FUS^{WT}	This paper	N/A
pTHMT/FUS$_{WT}$	Ref. (20)	N/A
U_{40} RNA: 5′- rUrUrU rUrUrU rUrUrU rUrUrU rUrUrU rUrUrU rUrUrU rUrUrU rUrUrU rU/3AmMO/-3′	IDT	N/A
Software and Algorithms		
ImageJ	Ref. (136)	https://imagej.nih.gov/ij/
GraphPad Prism	GraphPad	Version 9.1.1
MATLAB	Mathworks	
NIS-Elements Ar Package	Nikon	

GATCCAAGGCTGCTGCCCTGGATGTTCTT-3′; and 5′-CAGGGCGGATCCAAGTACCTTGCTTATATACTTGATACCCTG-3′. Truncated constructs were then shuttled into a Gateway entry vector, pDONR221-ccdB, using Gateway BP reactions (Invitrogen). H8-H16 was generated at this point using the following primer to introduce a stop codon at the end of H16: 3′-GGGGACCACTTTGTACAAGAAAGCTGGGTCCTAAGGCTGCATCTCTATACCCATTTG-5′. The entry clones were then used to shuttle Kapβ2 truncations into pAG416GAL-ccdB *via* Gateway LR reactions for yeast expression. FLAG-tagged constructs were created by using primers to add the following sequence upstream of the stop codon for each ORF: 5′-GACTACAAAGACGATGACGACAAG-3′.

To create plasmids for expression in mammalian cells, FUS and Kapβ2 were cloned into pEGFP-C1 and mCherry2-C1 (Addgene, #54563), respectively. The FUS ORFs were amplified with the following overhang sequences: 5′-GGACGAGCTGTACAAG-3′; 3′-GTAATCAGATCTGAGTCCGG-5′. Kapβ2 ORFs were amplified with the following overhang sequences: 5′-GGACGAGCTGTACAAGTCT-3′; 3′-CTCGAGATCTGAGTCCGG-5′. For both ORFs, the vector backbone was cut with

BspEI, and the linearized backbone and amplified inserts were purified using QIAquick Gel Extraction Kit (Qiagen) and assembled using Gibson cloning (NEB).

To create plasmids for the recombinant expression of Kapβ2 plasmids, Kapβ2 ORFs were cloned into a pE-SUMOpro Amp vector (LifeSensors) using the following strategy: first, the empty pE-SUMOpro Amp vector was cut using BsaI enzyme (NEB). ORFs were amplified with primers that added 5′-CGCGAACAGATTGGAGGT-3′ upstream of the start of the ORF and added 5′-CTAGAGGATCCGAATTC-3′ downstream of the end of the ORF. The cut vector and amplified ORFs were purified using a QIAquick Gel Extraction Kit (Qiagen) and assembled using Gibson cloning (NEB).

All constructs were confirmed by DNA sequencing.

Yeast strains and media

Yeast were the isogenic strain W303aΔ*hsp104* (94). The yeast strain W303aΔhsp104-pAG303GAL-FUS^{WT} and W303aΔhsp104-pAG303GAL-FUS^{WT}-GFP have been described previously (94, 97). Media was supplemented with 2% glucose, raffinose, or galactose as specified.

Yeast transformation and spotting assays

Yeast transformations were performed using standard PEG and lithium acetate procedures (132). For the spotting assays, yeast were grown to saturation in raffinose-supplemented dropout media overnight at 30 °C. The saturated overnight cultures were normalized to an A_{600} of 2.0 (A_{600nm} = 2.0) and serially diluted three-fold. A 96-bolt replicator tool (frogger) was used to spot the strains in duplicate onto both glucose and galactose dropout plates. These plates were grown at 30 °C and imaged after 72 h to assess suppression of FUS toxicity. Each spotting assay shown is representative of at least three biological replicates.

Western blots

For yeast cells, transformed Kapβ2 variants and controls were grown overnight in raffinose media. The overnight cultures were diluted to an A_{600} of 0.3 (A_{600nm} = 0.3) and grown in galactose-supplemented media at 30 °C for 5 h. Samples were then normalized to an A_{600} of 0.6 (A_{600nm} = 0.6) and centrifuged at 4000*g* for 5 min. The pelleted cells were resuspended in 0.1 M NaOH for 5 min and then pelleted again and resuspended in 1× SDS sample buffer. For HeLa cells, ∼2 to 2.5 × 10^5 cells were seeded and transfected with GFP-tagged FUS and either mCherry-tagged Kapβ2 variants or an empty vector expressing mCherry. After 24 h, cells were washed once with PBS, then resuspended in RIPA lysis buffer (150 mM NaCl, 1% Triton X-100, 1% sodium deoxycholate, 0.1% SDS, 25 mM Tris–HCl pH 7.6) supplemented with protease inhibitors and 1 mM PMSF. Cells were then sonicated and centrifuged at 4 °C for 10 min at 10,000*g*, and the cell lysate was mixed with 1× SDS sample buffer.

The samples were then boiled and separated by SDS-PAGE (4–20% gradient, Bio-Rad) and transferred to a PVDF membrane. The following primary antibodies were used: anti-FUS polyclonal (Bethyl Laboratories), anti-Kapβ2 monoclonal (Novus), anti-alpha Tubulin monoclonal (Abcam: ab184970 for yeast; ab6160 for human cells), anti-FLAG monoclonal (Sigma-Aldrich), anti-GFP polyclonal (Sigma-Aldrich), anti-mCherry polyclonal (Abcam). Three fluorescently labeled secondary antibodies were used: anti-rabbit (Li-Cor), anti-rat (Li-Cor), and anti-mouse (Li-Cor). Blots were imaged using a LI-COR Odyssey FC Imaging system.

HeLa cell culture and transfections

HeLa cells were maintained in Dulbecco's modified Eagle's medium, high glucose (Gibco) containing 10% fetal bovine serum (HyClone) and 1% penicillin-streptomycin (Gibco). Cells were plated in 6-well plates at a density of 2 to 2.5 × 10^5 cells/plate 24 h before transfection. Cells were transfected with 1 μg total DNA and 3 μl Lipofectamine 2000 (Invitrogen). Media was changed 4 h posttransfection to standard maintenance media, and cells were harvested for microscopy or Western blot 24 h posttransfection.

Fluorescence microscopy

For yeast microscopy, W303aΔhsp104-pAG303GAL-FUS^{WT}-GFP yeast were transformed with the indicated Kapβ2 variant or vector control. Microscopy samples were grown and induced as they were for immunoblotting. Prior to imaging, cells were treated with Hoechst 33342 stain (0.1 mg/ml). All cells were imaged at 100× magnification using a Leica-DMIRBE microscope or the EVOS M5000 Imaging System. Analysis of cells was performed in ImageJ (133). For each sample, at least 100 cells were quantified in at least three independent trials.

For HeLa cell microscopy, transfected HeLa cells were fixed with 2% formaldehyde for 30 min at room temperature, followed by treatment with Triton X-100 for 6 min to permeabilize cells. Coverslips were then assembled using VECTASHIELD Antifade Mounting Medium with DAPI (Vector Laboratories) and sealed before imaging. Images were taken at 100× magnification using the EVOS M5000 Imaging System (ThermoFisher) and processed using ImageJ (133). At least 100 cells were counted for each condition across three independent trials.

Protein purification

All proteins were expressed and purified from *Escherichia coli* BL21-CodonPlus(DE3)-RIL cells (Agilent) and purified under native conditions. GST-TEV-FUS^{WT} was purified as described (93). Briefly, *E. coli* cells were lysed by sonication on ice in PBS pH 7.4 with protease inhibitors (cOmplete, EDTA-free, Roche Applied Science). The protein was purified over Glutathione Sepharose 4 Fast Flow (GE Healthcare) and eluted from the beads using 50 mM Tris–HCl pH 8, 20 mM trehalose, and 20 mM glutathione. 6xHis-MBP-FUS was purified as described (20). Briefly, *E. coli* cells were lysed by sonication in lysis buffer (1 M KCl, 1 M Urea, 50 mM Tris–HCl pH 7.4, 10 mM imidazole, 1.5 mM β-mercaptoethanol, 1% NP-40, 5%

glycerol, supplemented with protease inhibitors). The protein was purified over a HisTrap HP column (GE), using an AKTA pure 25M FPLC system (GE), and was eluted using an imidazole gradient into elution buffer (1 M KCl, 1 M Urea, 50 mM Tris–HCl pH 7.4, 1.5 mM β-mercaptoethanol, 5% glycerol, 500 mM imidazole), and the appropriate fractions were pooled and stored in 30% glycerol at 4 °C.

To purify FL and truncated Kapβ2 proteins, *E. coli* cells transformed with the appropriate plasmid were grown at 37 °C in LB supplemented with 2% glucose. Once cells reached an A_{600} of ∼0.6, expression was induced overnight at 15 °C with 0.2 to 1.0 mM IPTG. Cells were pelleted and resuspended in binding buffer (50 mM Tris–HCl, pH 7.5, 100 mM NaCl, 20% glycerol, 10 mM imidazole, 2.5 mM β-mercaptoethanol, supplemented with protease inhibitors), then lysed by sonication. Cell lysate was separated by spinning at 16,000 rpm at 4 °C for 20 min. Cell lysate was then loaded onto Ni-NTA resin (Qiagen) and washed with binding buffer. Protein was eluted with elution buffer (50 mM Tris–HCl, pH 7.5, 100 mM NaCl, 20% glycerol, 200 mM imidazole, 2.5 mM β-mercaptoethanol) and buffer exchanged into a low imidazole buffer (20 mM imidazole pH 6.5, 75 mM NaCl, 2.5 mM β-mercaptoethanol, 20% glycerol). Protein was then cleaved at 30 °C overnight with Ulp1 at a 1:250 M ratio in an Eppendorf ThermoMixer shaking at 300 rpm. Cleaved protein product was then bound to fresh Ni-NTA resin, and flow-through was collected and further purified on a HiTrap Q HP column (GE) using buffer A (20 mM imidazole pH 6.5, 75 mM NaCl, 1 mM EDTA, 2 mM DTT, 20% glycerol) and buffer B (20 mM imidazole pH 6.5, 1 M NaCl, 1 mM EDTA, 2 mM DTT, 20% glycerol). Protein fractions were then concentrated, snap-frozen in liquid nitrogen, and stored at −80 °C.

FUS fibrillization assays

Spontaneous FUS fibrillization (*i.e.*, in the absence of preformed fibril seeds) was initiated as described previously (16). Briefly, 1 μg TEV protease was added to GST-TEV-FUS (3 μM) in FUS assembly buffer (50 mM Tris–HCl, pH 8, 200 mM trehalose, 1 mM DTT, and 20 mM glutathione) (37, 38, 93). Spontaneous FUS fibrillization reactions were incubated at 25 °C with or without the indicated concentration of each Kapβ2 variant, and turbidity was used to assess fibrillization by measuring absorbance at 395 nm. The absorbance was normalized to that of FUS plus buffer control to determine the relative extent of aggregation. Disaggregation assays were performed similarly, where FUS aggregation was initiated with TEV in the absence of Kapβ2. After 60 min of aggregation, equal volumes were added to each condition containing the appropriate ratios of buffer and Kapβ2 to reach the indicated final concentration.

To analyze data, the reading from the first timepoint was subtracted from every subsequent reading. Then, for each aggregation experiment, the maximum absorbance value for FUS alone was set as 100, and all other values were normalized to that standard by dividing the raw, background-subtracted value by the maximum value for FUS alone and multiplying by 100. For disaggregation experiments, the background-subtracted reading from the timepoint immediately before Kapβ2 addition was set to 100 for each condition, and subsequent readings were normalized to their own initial standard. For fibrillization assays, the area under the curve (AUC) for the first 90 min of fibrillization was used to calculate the IC_{50} by dividing the AUC for each condition by the AUC for FUS alone and multiplying by 100 to calculate a normalized percent aggregation. The same data treatment was used for disaggregation assays, where the AUC for the first 40 min after addition of Kapβ2 or buffer was used to calculate the EC_{50}. AUC, IC_{50}, and EC_{50} were calculated using GraphPad Prism by fitting data to a nonlinear regression using a normalized response and a variable slope.

Droplet assays

U_{40} RNA was labeled as described previously (20). Briefly, unlabeled amine-modified RNA was combined with 0.1 mg Cy3-NHS in 100 mM sodium bicarbonate for overnight labeling. The RNA was precipitated with ethanol twice and stored at −20 °C as 100 μM long-term and 1 μM working stocks.

Droplet reactions were performed essentially as described previously with a few modifications (20). Purified 6xHis-MBP-FUS was buffer-exchanged by concentrating FUS in Amicon filters (Millipore Sigma) and diluting with 20 mM Na2HPO4 pH 8.0. FUS (1 μM) was combined with unlabeled U40 RNA (1 μM) and Cy3-U40 (10 nM) in 1× cleavage buffer (100 mM NaCl, 50 mM Tris pH 7.4., 1 mM DTT, and 1 mM EDTA pH 8.0.). The phase separation reaction was initiated by adding 5 U Novex AcTEV protease, which cleaved the MBP and His tags from the FUS protein. Reactions (200 μl) were incubated for 4 h in 8-well Nunc Lab-Tek chambers (Thermo Scientific #155361). Brightfield and Cy3 fluorescence images were captured on a Nikon Ti Eclipse wide-field microscope. Purified Kapβ2 protein was prepared as a 10× concentrate (2.5–10 μM) in 1× cleavage buffer and diluted to 1× Kapβ2 (750 nM) in the phase separation reactions immediately after the 4-h timepoint.

Droplet area and number were quantified with a MATLAB script that used intensity thresholding to identify droplet regions of interest (ROIs) (21). We defined the area density as the sum of the area of all droplet ROIs divided by the total imaging area, which estimates the fraction of surface area covered by droplets. Therefore, the area density is unitless. The number of droplet ROIs and the area density of each image were determined for each replicate, which were then used to calculate the droplet statistics before and after Kapβ2 addition.

Data availability

All data are contained within the article.

Supporting information—This article contains supporting information.

Acknowledgments—We thank Katie Copley, Miriam Linsenmeier, JiaBei Lin, Zarin Tabassum, and Hana Odeh for feedback on the article and Oliver King for advice on statistics.

Author contributions—C. M. F., K. R., A. L., S. M., and J. S. conceptualization; C. M. F., K. R., A. L., S. M., and J. S. methodology; C. M. F., K. R., and A. L. validation; C. M. F. and K. R. formal analysis; C. M. F., K. R., and A. L. investigation; C. M. F., K. R., S. M., and J. S. resources; C. M. F. and K. R. data curation; C. M. F. and J. S. writing–original draft; C. M. F., K. R., A. L., S. M., and J. S. writing–review and editing; C. M. F., K. R., and J. S. visualization; C. M. F., S. M., and J. S. supervision; C. M. F., K. R., S. M., and J. S. funding acquisition; S. M. and J. S. project administration.

Funding and additional information—C. M. F. is supported by NIH grants T32GM008275 and F31NS111870. K. R. is supported by NIH grants F31NS113439 and T32GM007231. S. M. is funded by the NIH grants RF1AG071326 and RF1NS113636 and the NSF grant PHY-1430124 *via* the Center of Physics of Living Cells. J. S. is supported by grants from Target ALS, the ALS Association, the Office of the Assistant Secretary of Defense for Health Affairs through the Amyotrophic Lateral Sclerosis Research Program (W81XWH-20-1-0242), the G. Harold & Leila Y. Mathers Foundation, Sanofi, and NIH grants R01GM099836, R21AG061784, and R21AG065854. The content is solely the responsibility of the authors and does not necessarily represent the official views of the National Institutes of Health.

Conflict of interest—C. M. F., K. R., A. L., and S. M. have no interests to declare. J. S. is a consultant for Dewpoint Therapeutics, ADRx, and Neumora. J.S. is a shareholder and advisor for Confluence Therapeutics.

Abbreviations—The abbreviations used are: AAV, adeno-associated virus; ALS, amyotrophic lateral sclerosis; AUC, area under the curve; FL, full-length; FTD, frontotemporal dementia; HEAT, Huntington, Elongation factor 3, A subunit of protein phosphatase 2A, and Tor1 kinase; Kapβ2, Karyopherin-β2; MSP, multisystem proteinopathy; NIR, nuclear-import receptor; PrLD, prion-like domain; PY-NLS, proline-tyrosine nuclear localization signal; RBP, RNA-binding protein; ROI, region of interest.

References

1. Lee, B. J., Cansizoglu, A. E., Suel, K. E., Louis, T. H., Zhang, Z., and Chook, Y. M. (2006) Rules for nuclear localization sequence recognition by Karyopherin beta 2. *Cell* **126**, 543–558
2. Soniat, M., and Chook, Y. M. (2015) Nuclear localization signals for four distinct Karyopherin-beta nuclear import systems. *Biochem. J.* **468**, 353–362
3. Wing, C. E., Fung, H. Y. J., and Chook, Y. M. (2022) Karyopherin-mediated nucleocytoplasmic transport. *Nat. Rev. Mol. Cell Biol.* **23**, 307–328
4. Xu, D., Farmer, A., and Chook, Y. M. (2010) Recognition of nuclear targeting signals by Karyopherin-beta proteins. *Curr. Opin. Struct. Biol.* **20**, 782–790
5. Gorlich, D., Pante, N., Kutay, U., Aebi, U., and Bischoff, F. R. (1996) Identification of different roles for RanGDP and RanGTP in nuclear protein import. *EMBO J.* **15**, 5584–5594
6. Guo, L., Fare, C. M., and Shorter, J. (2019) Therapeutic dissolution of aberrant phases by nuclear-import receptors. *Trends Cell Biol.* **29**, 308–322
7. Chook, Y. M., and Blobel, G. (1999) Structure of the nuclear transport complex Karyopherin-beta2-Ran x GppNHp. *Nature* **399**, 230–237
8. Nakielny, S., and Dreyfuss, G. (1998) Import and export of the nuclear protein import receptor transportin by a mechanism independent of GTP hydrolysis. *Curr. Biol.* **8**, 89–95
9. Nakielny, S., Siomi, M. C., Siomi, H., Michael, W. M., Pollard, V., and Dreyfuss, G. (1996) Transportin: nuclear transport receptor of a novel nuclear protein import pathway. *Exp. Cell Res.* **229**, 261–266
10. Siomi, M. C., Eder, P. S., Kataoka, N., Wan, L., Liu, Q., and Dreyfuss, G. (1997) Transportin-mediated nuclear import of heterogeneous nuclear RNP proteins. *J. Cell Biol.* **138**, 1181–1192
11. Pollard, V. W., Michael, W. M., Nakielny, S., Siomi, M. C., Wang, F., and Dreyfuss, G. (1996) A novel receptor-mediated nuclear protein import pathway. *Cell* **86**, 985–994
12. Soniat, M., and Chook, Y. M. (2016) Karyopherin-β2 recognition of a PY-NLS variant that lacks the proline-tyrosine motif. *Structure* **24**, 1802–1809
13. Süel, K. E., Gu, H., and Chook, Y. M. (2008) Modular organization and combinatorial energetics of proline-tyrosine nuclear localization signals. *PLoS Biol.* **6**, e137
14. Zhang, Z. C., and Chook, Y. M. (2012) Structural and energetic basis of ALS-causing mutations in the atypical proline-tyrosine nuclear localization signal of the fused in sarcoma protein (FUS). *Proc. Natl. Acad. Sci. U. S. A.* **109**, 12017–12021
15. Bonifaci, N., Moroianu, J., Radu, A., and Blobel, G. (1997) Karyopherin beta2 mediates nuclear import of a mRNA binding protein. *Proc. Natl. Acad. Sci. U. S. A.* **94**, 5055–5060
16. Guo, L., Kim, H. J., Wang, H., Monaghan, J., Freyermuth, F., Sung, J. C., *et al.* (2018) Nuclear-import receptors reverse aberrant phase transitions of RNA-binding proteins with prion-like domains. *Cell* **173**, 677–692.e20
17. Hofweber, M., Hutten, S., Bourgeois, B., Spreitzer, E., Niedner-Boblenz, A., Schifferer, M., *et al.* (2018) Phase separation of FUS is suppressed by its nuclear import receptor and arginine methylation. *Cell* **173**, 706–719.e13
18. Qamar, S., Wang, G., Randle, S. J., Ruggeri, F. S., Varela, J. A., Lin, J. Q., *et al.* (2018) FUS phase separation is modulated by a molecular chaperone and methylation of arginine cation-pi interactions. *Cell* **173**, 720–734.e15
19. Yoshizawa, T., Ali, R., Jiou, J., Fung, H. Y. J., Burke, K. A., Kim, S. J., *et al.* (2018) Nuclear import receptor inhibits phase separation of FUS through binding to multiple sites. *Cell* **173**, 693–705.e22
20. Niaki, A. G., Sarkar, J., Cai, X., Rhine, K., Vidaurre, V., Guy, B., *et al.* (2020) Loss of dynamic RNA interaction and aberrant phase separation induced by two distinct types of ALS/FTD-linked FUS mutations. *Mol. Cell* **77**, 82–94.e4
21. Rhine, K., Dasovich, M., Yoniles, J., Badiee, M., Skanchy, S., Ganser, L. R., *et al.* (2022) Poly(ADP-ribose) drives condensation of FUS via a transient interaction. *Mol. Cell* **82**, 969–985.e11
22. Baade, I., Hutten, S., Sternburg, E. L., Porschke, M., Hofweber, M., Dormann, D., *et al.* (2021) The RNA-binding protein FUS is chaperoned and imported into the nucleus by a network of import receptors. *J. Biol. Chem.* **296**, 100659
23. Gonzalez, A., Mannen, T., Cagatay, T., Fujiwara, A., Matsumura, H., Niesman, A. B., *et al.* (2021) Mechanism of Karyopherin-beta2 binding and nuclear import of ALS variants FUS(P525L) and FUS(R495X). *Sci. Rep.* **11**, 3754
24. Rhine, K., Makurath, M. A., Liu, J., Skanchy, S., Lopez, C., Catalan, K. F., *et al.* (2020) ALS/FTLD-linked mutations in FUS glycine residues cause accelerated gelation and reduced interactions with wild-type FUS. *Mol. Cell* **80**, 666–681.e8
25. Darling, A. L., and Shorter, J. (2021) Combating deleterious phase transitions in neurodegenerative disease. *Biochim. Biophys. Acta Mol. Cell Res.* **1868**, 118984
26. Fare, C. M., and Shorter, J. (2021) (Dis)Solving the problem of aberrant protein states. *Dis. Model. Mech.* **14**, dmm048983
27. Odeh, H. M., Fare, C. M., and Shorter, J. (2022) Nuclear-import receptors counter deleterious phase transitions in neurodegenerative disease. *J. Mol. Biol.* **434**, 167220
28. Portz, B., Lee, B. L., and Shorter, J. (2021) FUS and TDP-43 phases in health and disease. *Trends Biochem. Sci.* **46**, 550–563

29. Fridell, R. A., Truant, R., Thorne, L., Benson, R. E., and Cullen, B. R. (1997) Nuclear import of hnRNP A1 is mediated by a novel cellular cofactor related to karyopherin-beta. *J. Cell Sci.* **110**, 1325–1331
30. King, O. D., Gitler, A. D., and Shorter, J. (2012) The tip of the iceberg: RNA-binding proteins with prion-like domains in neurodegenerative disease. *Brain Res.* **1462**, 61–80
31. Li, Y. R., King, O. D., Shorter, J., and Gitler, A. D. (2013) Stress granules as crucibles of ALS pathogenesis. *J. Cell Biol.* **201**, 361–372
32. Cushman, M., Johnson, B. S., King, O. D., Gitler, A. D., and Shorter, J. (2010) Prion-like disorders: blurring the divide between transmissibility and infectivity. *J. Cell Sci.* **123**, 1191–1201
33. Gitler, A. D., and Shorter, J. (2011) RNA-binding proteins with prion-like domains in ALS and FTLD-U. *Prion* **5**, 179–187
34. March, Z. M., King, O. D., and Shorter, J. (2016) Prion-like domains as epigenetic regulators, scaffolds for subcellular organization, and drivers of neurodegenerative disease. *Brain Res.* **1647**, 9–18
35. Harrison, A. F., and Shorter, J. (2017) RNA-binding proteins with prion-like domains in health and disease. *Biochem. J.* **474**, 1417–1438
36. Kapeli, K., Martinez, F. J., and Yeo, G. W. (2017) Genetic mutations in RNA-binding proteins and their roles in ALS. *Hum. Genet.* **136**, 1193–1214
37. Couthouis, J., Hart, M. P., Erion, R., King, O. D., Diaz, Z., Nakaya, T., *et al.* (2012) Evaluating the role of the FUS/TLS-related gene EWSR1 in amyotrophic lateral sclerosis. *Hum. Mol. Genet.* **21**, 2899–2911
38. Couthouis, J., Hart, M. P., Shorter, J., DeJesus-Hernandez, M., Erion, R., Oristano, R., *et al.* (2011) A yeast functional screen predicts new candidate ALS disease genes. *Proc. Natl. Acad. Sci. U. S. A.* **108**, 20881–20890
39. Kim, H. J., Kim, N. C., Wang, Y. D., Scarborough, E. A., Moore, J., Diaz, Z., *et al.* (2013) Mutations in prion-like domains in hnRNPA2B1 and hnRNPA1 cause multisystem proteinopathy and ALS. *Nature* **495**, 467–473
40. Beijer, D., Kim, H. J., Guo, L., O'Donovan, K., Mademan, I., Deconinck, T., *et al.* (2021) Characterization of HNRNPA1 mutations defines diversity in pathogenic mechanisms and clinical presentation. *JCI Insight* **6**, e148363
41. Kim, H. J., Mohassel, P., Donkervoort, S., Guo, L., O'Donovan, K., Coughlin, M., *et al.* (2022) Heterozygous frameshift variants in HNRNPA2B1 cause early-onset oculopharyngeal muscular dystrophy. *Nat. Commun.* **13**, 2306
42. Couthouis, J., Raphael, A. R., Daneshjou, R., and Gitler, A. D. (2014) Targeted exon capture and sequencing in sporadic amyotrophic lateral sclerosis. *PLoS Genet.* **10**, e1004704
43. Blokhuis, A. M., Groen, E. J., Koppers, M., van den Berg, L. H., and Pasterkamp, R. J. (2013) Protein aggregation in amyotrophic lateral sclerosis. *Acta Neuropathol.* **125**, 777–794
44. Ito, D., Hatano, M., and Suzuki, N. (2017) RNA binding proteins and the pathological cascade in ALS/FTD neurodegeneration. *Sci. Transl. Med.* **9**, eaah5436
45. Mackenzie, I. R., Rademakers, R., and Neumann, M. (2010) TDP-43 and FUS in amyotrophic lateral sclerosis and frontotemporal dementia. *Lancet Neurol.* **9**, 995–1007
46. Neumann, M., Rademakers, R., Roeber, S., Baker, M., Kretzschmar, H. A., and Mackenzie, I. R. (2009) A new subtype of frontotemporal lobar degeneration with FUS pathology. *Brain* **132**, 2922–2931
47. Tyzack, G. E., Luisier, R., Taha, D. M., Neeves, J., Modic, M., Mitchell, J. S., *et al.* (2019) Widespread FUS mislocalization is a molecular hallmark of amyotrophic lateral sclerosis. *Brain* **142**, 2572–2580
48. Vance, C., Scotter, E. L., Nishimura, A. L., Troakes, C., Mitchell, J. C., Kathe, C., *et al.* (2013) ALS mutant FUS disrupts nuclear localization and sequesters wild-type FUS within cytoplasmic stress granules. *Hum. Mol. Genet.* **22**, 2676–2688
49. Kwiatkowski, T. J., Jr., Bosco, D. A., Leclerc, A. L., Tamrazian, E., Vanderburg, C. R., Russ, C., *et al.* (2009) Mutations in the FUS/TLS gene on chromosome 16 cause familial amyotrophic lateral sclerosis. *Science* **323**, 1205–1208
50. Hoell, J. I., Larsson, E., Runge, S., Nusbaum, J. D., Duggimpudi, S., Farazi, T. A., *et al.* (2011) RNA targets of wild-type and mutant FET family proteins. *Nat. Struct. Mol. Biol.* **18**, 1428–1431
51. Humphrey, J., Birsa, N., Milioto, C., McLaughlin, M., Ule, A. M., Robaldo, D., *et al.* (2020) FUS ALS-causative mutations impair FUS autoregulation and splicing factor networks through intron retention. *Nucleic Acids Res.* **48**, 6889–6905
52. Kamelgarn, M., Chen, J., Kuang, L., Jin, H., Kasarskis, E. J., and Zhu, H. (2018) ALS mutations of FUS suppress protein translation and disrupt the regulation of nonsense-mediated decay. *Proc. Natl. Acad. Sci. U. S. A.* **115**, E11904–E11913
53. Korobeynikov, V. A., Lyashchenko, A. K., Blanco-Redondo, B., Jafar-Nejad, P., and Shneider, N. A. (2022) Antisense oligonucleotide silencing of FUS expression as a therapeutic approach in amyotrophic lateral sclerosis. *Nat. Med.* **28**, 104–116
54. Murakami, T., Qamar, S., Lin, J. Q., Schierle, G. S., Rees, E., Miyashita, A., *et al.* (2015) ALS/FTD mutation-induced phase transition of FUS liquid droplets and reversible hydrogels into irreversible hydrogels impairs RNP granule function. *Neuron* **88**, 678–690
55. Tsai, Y. L., Coady, T. H., Lu, L., Zheng, D., Alland, I., Tian, B., *et al.* (2020) ALS/FTD-associated protein FUS induces mitochondrial dysfunction by preferentially sequestering respiratory chain complex mRNAs. *Genes Dev.* **34**, 785–805
56. Verdile, V., De Paola, E., and Paronetto, M. P. (2019) Aberrant phase transitions: side effects and novel therapeutic strategies in human disease. *Front. Genet.* **10**, 173
57. Winklhofer, K. F., Tatzelt, J., and Haass, C. (2008) The two faces of protein misfolding: gain- and loss-of-function in neurodegenerative diseases. *EMBO J.* **27**, 336–349
58. Coady, T. H., and Manley, J. L. (2015) ALS mutations in TLS/FUS disrupt target gene expression. *Genes Dev.* **29**, 1696–1706
59. Gomes, E., and Shorter, J. (2019) The molecular language of membraneless organelles. *J. Biol. Chem.* **294**, 7115–7127
60. Fare, C. M., Villani, A., Drake, L. E., and Shorter, J. (2021) Higher-order organization of biomolecular condensates. *Open Biol.* **11**, 210137
61. Levone, B. R., Lenzken, S. C., Antonaci, M., Maiser, A., Rapp, A., Conte, F., *et al.* (2021) FUS-dependent liquid-liquid phase separation is important for DNA repair initiation. *J. Cell Biol.* **220**, e202008030
62. Gasset-Rosa, F., Lu, S., Yu, H., Chen, C., Melamed, Z., Guo, L., *et al.* (2019) Cytoplasmic TDP-43 de-mixing independent of stress granules drives inhibition of nuclear import, loss of nuclear TDP-43, and cell death. *Neuron* **102**, 339–357.e7
63. Molliex, A., Temirov, J., Lee, J., Coughlin, M., Kanagaraj, A. P., Kim, H. J., *et al.* (2015) Phase separation by low complexity domains promotes stress granule assembly and drives pathological fibrillization. *Cell* **163**, 123–133
64. Hallegger, M., Chakrabarti, A. M., Lee, F. C. Y., Lee, B. L., Amalietti, A. G., Odeh, H. M., *et al.* (2021) TDP-43 condensation properties specify its RNA-binding and regulatory repertoire. *Cell* **184**, 4680–4696.e22
65. Kato, M., Han, T. W., Xie, S., Shi, K., Du, X., Wu, L. C., *et al.* (2012) Cell-free formation of RNA granules: low complexity sequence domains form dynamic fibers within hydrogels. *Cell* **149**, 753–767
66. Buchan, J. R., and Parker, R. (2009) Eukaryotic stress granules: the ins and outs of translation. *Mol. Cell* **36**, 932–941
67. Mahboubi, H., and Stochaj, U. (2017) Cytoplasmic stress granules: dynamic modulators of cell signaling and disease. *Biochim. Biophys. Acta Mol. Basis Dis.* **1863**, 884–895
68. Protter, D. S. W., and Parker, R. (2016) Principles and properties of stress granules. *Trends Cell Biol.* **26**, 668–679
69. Wolozin, B., and Ivanov, P. (2019) Stress granules and neurodegeneration. *Nat. Rev. Neurosci.* **20**, 649–666
70. Patel, A., Lee, H. O., Jawerth, L., Maharana, S., Jahnel, M., Hein, M. Y., *et al.* (2015) A liquid-to-solid phase transition of the ALS protein FUS accelerated by disease mutation. *Cell* **162**, 1066–1077
71. Reineke, L. C., and Neilson, J. R. (2019) Differences between acute and chronic stress granules, and how these differences may impact function in human disease. *Biochem. Pharmacol.* **162**, 123–131

72. Zhang, P., Fan, B., Yang, P., Temirov, J., Messing, J., Kim, H. J., *et al.* (2019) Chronic optogenetic induction of stress granules is cytotoxic and reveals the evolution of ALS-FTD pathology. *Elife* **8**, e39578
73. Mann, J. R., Gleixner, A. M., Mauna, J. C., Gomes, E., DeChellis-Marks, M. R., Needham, P. G., *et al.* (2019) RNA binding antagonizes neurotoxic phase transitions of TDP-43. *Neuron* **102**, 321–338.e8
74. Hutten, S., Usluer, S., Bourgeois, B., Simonetti, F., Odeh, H. M., Fare, C. M., *et al.* (2020) Nuclear import receptors directly bind to arginine-rich dipeptide repeat proteins and suppress their pathological interactions. *Cell Rep.* **33**, 108538
75. Jovicic, A., Mertens, J., Boeynaems, S., Bogaert, E., Chai, N., Yamada, S. B., *et al.* (2015) Modifiers of C9orf72 dipeptide repeat toxicity connect nucleocytoplasmic transport defects to FTD/ALS. *Nat. Neurosci.* **18**, 1226–1229
76. Freibaum, B. D., Lu, Y., Lopez-Gonzalez, R., Kim, N. C., Almeida, S., Lee, K. H., *et al.* (2015) GGGGCC repeat expansion in C9orf72 compromises nucleocytoplasmic transport. *Nature* **525**, 129–133
77. Hayes, L. R., Duan, L., Bowen, K., Kalab, P., and Rothstein, J. D. (2020) C9orf72 arginine-rich dipeptide repeat proteins disrupt karyopherin-mediated nuclear import. *Elife* **9**, e51685
78. [preprint] Cicardi, M., Kankate, V., Sriramoji, S., Krishnamurthy, K., Markandaiah, S., Verdone, B., *et al.* (2022) Kapβ2 is a modifier of the C9orf72-linked glycine-arginine dipeptide neurotoxicity. *bioRxiv*. https://doi.org/10.1101/2022.09.30.510384
79. Conte, A., Lattante, S., Zollino, M., Marangi, G., Luigetti, M., Del Grande, A., *et al.* (2012) P525L FUS mutation is consistently associated with a severe form of juvenile amyotrophic lateral sclerosis. *Neuromuscul. Disord.* **22**, 73–75
80. Corcia, P., Danel, V., Lacour, A., Beltran, S., Andres, C., Couratier, P., *et al.* (2017) A novel mutation of the C-terminal amino acid of FUS (Y526C) strengthens FUS gene as the most frequent genetic factor in aggressive juvenile ALS. *Amyotroph. Lateral Scler. Frontotemporal Degener.* **18**, 298–301
81. Niu, C., Zhang, J., Gao, F., Yang, L., Jia, M., Zhu, H., *et al.* (2012) FUS-NLS/transportin 1 complex structure provides insights into the nuclear targeting mechanism of FUS and the implications in ALS. *PLoS One* **7**, e47056
82. Chook, Y. M., and Blobel, G. (2001) Karyopherins and nuclear import. *Curr. Opin. Struct. Biol.* **11**, 703–715
83. Cansizoglu, A. E., Lee, B. J., Zhang, Z. C., Fontoura, B. M., and Chook, Y. M. (2007) Structure-based design of a pathway-specific nuclear import inhibitor. *Nat. Struct. Mol. Biol.* **14**, 452–454
84. Yoshimura, S. H., and Hirano, T. (2016) HEAT repeats – versatile arrays of amphiphilic helices working in crowded environments? *J. Cell Sci.* **129**, 3963–3970
85. Fukuhara, N., Fernandez, E., Ebert, J., Conti, E., and Svergun, D. (2004) Conformational variability of nucleo-cytoplasmic transport factors. *J. Biol. Chem.* **279**, 2176–2181
86. Cansizoglu, A. E., and Chook, Y. M. (2007) Conformational heterogeneity of Karyopherin beta2 is segmental. *Structure* **15**, 1431–1441
87. Iijima, M., Suzuki, M., Tanabe, A., Nishimura, A., and Yamada, M. (2006) Two motifs essential for nuclear import of the hnRNP A1 nucleocytoplasmic shuttling sequence M9 core. *FEBS Lett.* **580**, 1365–1370
88. Shorter, J., and Southworth, D. R. (2019) Spiraling in control: structures and mechanisms of the Hsp104 disaggregase. *Cold Spring Harb. Perspect. Biol.* **11**, a034033
89. Erives, A. J., and Fassler, J. S. (2015) Metabolic and chaperone gene loss marks the origin of animals: evidence for Hsp104 and Hsp78 chaperones sharing mitochondrial enzymes as clients. *PLoS One* **10**, e0117192
90. Shorter, J. (2008) Hsp104: a weapon to combat diverse neurodegenerative disorders. *Neurosignals* **16**, 63–74
91. Sweeny, E. A., and Shorter, J. (2016) Mechanistic and structural insights into the prion-disaggregase activity of Hsp104. *J. Mol. Biol.* **428**, 1870–1885
92. Ju, S., Tardiff, D. F., Han, H., Divya, K., Zhong, Q., Maquat, L. E., *et al.* (2011) A yeast model of FUS/TLS-dependent cytotoxicity. *PLoS Biol.* **9**, e1001052
93. Sun, Z., Diaz, Z., Fang, X., Hart, M. P., Chesi, A., Shorter, J., *et al.* (2011) Molecular determinants and genetic modifiers of aggregation and toxicity for the ALS disease protein FUS/TLS. *PLoS Biol.* **9**, e1000614
94. Jackrel, M. E., DeSantis, M. E., Martinez, B. A., Castellano, L. M., Stewart, R. M., Caldwell, K. A., *et al.* (2014) Potentiated Hsp104 variants antagonize diverse proteotoxic misfolding events. *Cell* **156**, 170–182
95. Sabatelli, M., Moncada, A., Conte, A., Lattante, S., Marangi, G., Luigetti, M., *et al.* (2013) Mutations in the 3' untranslated region of FUS causing FUS overexpression are associated with amyotrophic lateral sclerosis. *Hum. Mol. Genet.* **22**, 4748–4755
96. Dini Modigliani, S., Morlando, M., Errichelli, L., Sabatelli, M., and Bozzoni, I. (2014) An ALS-associated mutation in the FUS 3'-UTR disrupts a microRNA-FUS regulatory circuitry. *Nat. Commun.* **5**, 4335
97. Jackrel, M. E., and Shorter, J. (2014) Potentiated Hsp104 variants suppress toxicity of diverse neurodegenerative disease-linked proteins. *Dis. Model. Mech.* **7**, 1175–1184
98. Jackrel, M. E., Yee, K., Tariq, A., Chen, A. I., and Shorter, J. (2015) Disparate mutations confer therapeutic gain of Hsp104 function. *ACS Chem. Biol.* **10**, 2672–2679
99. Tariq, A., Lin, J., Jackrel, M. E., Hesketh, C. D., Carman, P. J., Mack, K. L., *et al.* (2019) Mining disaggregase sequence space to safely counter TDP-43, FUS, and alpha-synuclein proteotoxicity. *Cell Rep.* **28**, 2080–2095.e6
100. Yasuda, K., Clatterbuck-Soper, S. F., Jackrel, M. E., Shorter, J., and Mili, S. (2017) FUS inclusions disrupt RNA localization by sequestering kinesin-1 and inhibiting microtubule detyrosination. *J. Cell Biol.* **216**, 1015–1034
101. Daigle, J. G., Lanson, N. A., Jr., Smith, R. B., Casci, I., Maltare, A., Monaghan, J., *et al.* (2013) RNA-binding ability of FUS regulates neurodegeneration, cytoplasmic mislocalization and incorporation into stress granules associated with FUS carrying ALS-linked mutations. *Hum. Mol. Genet.* **22**, 1193–1205
102. Barmada, S. J., Ju, S., Arjun, A., Batarse, A., Archbold, H. C., Peisach, D., *et al.* (2015) Amelioration of toxicity in neuronal models of amyotrophic lateral sclerosis by hUPF1. *Proc. Natl. Acad. Sci. U. S. A.* **112**, 7821–7826
103. Tariq, A., Lin, J., Noll, M. M., Torrente, M. P., Mack, K. L., Murillo, O. H., *et al.* (2018) Potentiating Hsp104 activity via phosphomimetic mutations in the middle domain. *FEMS Yeast Res.* **18**, foy042
104. Dian, C., Bernaudat, F., Langer, K., Oliva, M. F., Fornerod, M., Schoehn, G., *et al.* (2013) Structure of a truncation mutant of the nuclear export factor CRM1 provides insights into the auto-inhibitory role of its C-terminal helix. *Structure* **21**, 1338–1349
105. Tsytlonok, M., Craig, P. O., Sivertsson, E., Serquera, D., Perrett, S., Best, R. B., *et al.* (2013) Complex energy landscape of a giant repeat protein. *Structure* **21**, 1954–1965
106. Robinson, E., Shorter, J., and Guo, L. (2020) Karyopherin-beta2 inhibits and reverses aggregation and liquid-liquid phase separation of the ALS/FTD-associated protein FUS. *Bio Protoc.* **10**, e3725
107. Yang, L., Gal, J., Chen, J., and Zhu, H. (2014) Self-assembled FUS binds active chromatin and regulates gene transcription. *Proc. Natl. Acad. Sci. U. S. A.* **111**, 17809–17814
108. Reber, S., Jutzi, D., Lindsay, H., Devoy, A., Mechtersheimer, J., Levone, B. R., *et al.* (2021) The phase separation-dependent FUS interactome reveals nuclear and cytoplasmic function of liquid-liquid phase separation. *Nucleic Acids Res.* **49**, 7713–7731
109. Mallet, P. L., and Bachand, F. (2013) A proline-tyrosine nuclear localization signal (PY-NLS) is required for the nuclear import of fission yeast PAB2, but not of human PABPN1. *Traffic* **14**, 282–294
110. Sweeny, E. A., Jackrel, M. E., Go, M. S., Sochor, M. A., Razzo, B. M., DeSantis, M. E., *et al.* (2015) The Hsp104 N-terminal domain enables disaggregase plasticity and potentiation. *Mol. Cell* **57**, 836–849
111. Bayliss, R., Littlewood, T., and Stewart, M. (2000) Structural basis for the interaction between FxFG nucleoporin repeats and importin-beta in nuclear trafficking. *Cell* **102**, 99–108
112. Bednenko, J., Cingolani, G., and Gerace, L. (2003) Importin beta contains a COOH-terminal nucleoporin binding region important for nuclear transport. *J. Cell Biol.* **162**, 391–401

113. Chi, N. C., and Adam, S. A. (1997) Functional domains in nuclear import factor p97 for binding the nuclear localization sequence receptor and the nuclear pore. *Mol. Biol. Cell* **8**, 945–956
114. Kutay, U., Izaurralde, E., Bischoff, F. R., Mattaj, I. W., and Gorlich, D. (1997) Dominant-negative mutants of importin-beta block multiple pathways of import and export through the nuclear pore complex. *EMBO J.* **16**, 1153–1163
115. [preprint] Thomas, L., Askjaer, P., and Seydoux, G. (2022) Multiple mechanisms prevent ectopic condensation of FG nucleoporins in the cytoplasm. *bioRxiv*. https://doi.org/10.1101/2022.08.22.504855
116. Chook, Y. M., Jung, A., Rosen, M. K., and Blobel, G. (2002) Uncoupling Kapbeta2 substrate dissociation and ran binding. *Biochemistry* **41**, 6955–6966
117. Dormann, D., Madl, T., Valori, C. F., Bentmann, E., Tahirovic, S., Abou-Ajram, C., *et al.* (2012) Arginine methylation next to the PY-NLS modulates transportin binding and nuclear import of FUS. *EMBO J.* **31**, 4258–4275
118. Dormann, D., Rodde, R., Edbauer, D., Bentmann, E., Fischer, I., Hruscha, A., *et al.* (2010) ALS-associated fused in sarcoma (FUS) mutations disrupt transportin-mediated nuclear import. *EMBO J.* **29**, 2841–2857
119. Sproviero, W., La Bella, V., Mazzei, R., Valentino, P., Rodolico, C., Simone, I. L., *et al.* (2012) FUS mutations in sporadic amyotrophic lateral sclerosis: clinical and genetic analysis. *Neurobiol. Aging* **33**, 837 e831–e835
120. Liu, Q., Shu, S., Wang, R. R., Liu, F., Cui, B., Guo, X. N., *et al.* (2016) Whole-exome sequencing identifies a missense mutation in hnRNPA1 in a family with flail arm ALS. *Neurology* **87**, 1763–1769
121. Naruse, H., Ishiura, H., Mitsui, J., Date, H., Takahashi, Y., Matsukawa, T., *et al.* (2018) Molecular epidemiological study of familial amyotrophic lateral sclerosis in Japanese population by whole-exome sequencing and identification of novel HNRNPA1 mutation. *Neurobiol. Aging* **61**, 255. e9–255.e16
122. Carey, J. L., and Guo, L. (2022) Liquid-liquid phase separation of TDP-43 and FUS in physiology and pathology of neurodegenerative diseases. *Front. Mol. Biosci.* **9**, 826719
123. Kuzmin, D. A., Shutova, M. V., Johnston, N. R., Smith, O. P., Fedorin, V. V., Kukushkin, Y. S., *et al.* (2021) The clinical landscape for AAV gene therapies. *Nat. Rev. Drug Discov.* **20**, 173–174
124. Au, H. K. E., Isalan, M., and Mielcarek, M. (2021) Gene therapy advances: a meta-analysis of AAV usage in clinical settings. *Front. Med.* **8**, 809118
125. Mendell, J. R., Al-Zaidy, S. A., Rodino-Klapac, L. R., Goodspeed, K., Gray, S. J., Kay, C. N., *et al.* (2021) Current clinical applications of in vivo gene therapy with AAVs. *Mol. Ther.* **29**, 464–488
126. Wu, Z., Yang, H., and Colosi, P. (2010) Effect of genome size on AAV vector packaging. *Mol. Ther.* **18**, 80–86
127. Marrone, L., Marchi, P. M., and Azzouz, M. (2022) Circumventing the packaging limit of AAV-mediated gene replacement therapy for neurological disorders. *Expert Opin. Biol. Ther.* **22**, 1163–1176
128. Kim, H. J., and Taylor, J. P. (2017) Lost in transportation: nucleocytoplasmic transport defects in ALS and other neurodegenerative diseases. *Neuron* **96**, 285–297
129. Moore, S., Rabichow, B. E., and Sattler, R. (2020) The hitchhiker's guide to nucleocytoplasmic trafficking in neurodegeneration. *Neurochem. Res.* **45**, 1306–1327
130. Fallini, C., Khalil, B., Smith, C. L., and Rossoll, W. (2020) Traffic jam at the nuclear pore: all roads lead to nucleocytoplasmic transport defects in ALS/FTD. *Neurobiol. Dis.* **140**, 104835
131. Shubina-Oleinik, O., Nist-Lund, C., French, C., Rockowitz, S., Shearer, A. E., and Holt, J. R. (2021) Dual-vector gene therapy restores cochlear amplification and auditory sensitivity in a mouse model of DFNB16 hearing loss. *Sci. Adv.* **7**, eabi7629
132. Gietz, R. D., and Schiestl, R. H. (2007) High-efficiency yeast transformation using the LiAc/SS carrier DNA/PEG method. *Nat. Protoc.* **2**, 31–34
133. Schindelin, J., Arganda-Carreras, I., Frise, E., Kaynig, V., Longair, M., Pietzsch, T., *et al.* (2012) Fiji: an open-source platform for biological-image analysis. *Nat. Methods* **9**, 676–682
134. Schirmer, E. C., Homann, O. R., Kowal, A. S., and Lindquist, S. (2004) Dominant gain-of-function mutations in Hsp104p reveal crucial roles for the middle region. *Mol. Biol. Cell* **15**, 2061–2072
135. Cormack, B. P., Valdivia, R. H., and Falkow, S. (1996) FACS-optimized mutants of the green fluorescent protein (GFP). *Gene* **173**, 33–38
136. Schneider, C. A., Rasband, W. S., and Eliceiri, K. W. (2012) NIH image to ImageJ: 25 years of image analysis. *Nat. Methods* **9**, 671–675